ADDIS ABABA UNIVERSITY

SCHOOL OF GRADUATE STUDIES

THERMODYNAMICS OF THE METAL VACANCY IN ^{111}In DOPED ZnSe

By

MESFIN TSIGE

MARCH 1994

ADDIS ABABA

THERMODYNAMICS OF THE METAL VACANCY IN ^{111}In DOPED ZnSe

By

MESFIN TSIGE

A THESIS SUBMITTED TO

THE SCHOOL OF GRADUATE STUDIES

ADDIS ABABA UNIVERSITY

IN PARTIAL FULFILMENT

OF THE REQUIREMENT FOR THE DEGREE OF

MASTER OF SCIENCE IN PHYSICS

MARCH 1994

ADDIS ABABA

ACKNOWLEDGEMENTS

I am greatly indebted to my advisor Prof. Dr. Thomas Wichert for his constant assistance, invaluable guidance and friendly encouragement without any reservation during the whole period of my research work at the University of Saarbrüken, Germany.

I would like to express my due thanks to the research group led by Prof. Dr. Thomas Wichert for arranging and executing many diffusions and perturbed angular correlation experiments and for stimulating discussions on the interpretation of the data. I am particularly grateful to Dr. H. Wolf and Mr. E. Singer for their continued follow up of the research work. Also, many thanks to Messrs U. Hornauer, U. Ott, St. Lauer, R. Lermn, T. Filz, V. Ostheimer and Dr. Th. Krings whose valuable suggestions and useful advice accounted a lot when I faced problems.

It is my pleasure to express my heartfelt gratitude to my advisor and instructor Dr. I. M. Kashirski, Addis Ababa University, Ethiopia, for his constructive criticisms and comments.

On behalf of the Addis Ababa university, I want to extend my appreciation to the Deutscher Akademischer Austauschdienst (German Academic Exchange Service) - DAAD - for the financial support I received during my stay in Germany, without which the work would not have been possible. My thanks are also due to Dr. F. Dworschak who spent much of his precious time looking for a qualified and appropriate advisor in the area I proposed to work the research. I wish also to express my gratitude to Mrs. Wichert and Mrs. I . Micheals for their co-operation in smoothening down acute problems.

Finally, I would like to extend my deepest thanks and appreciation to Ato Bantikassegn Workalemahu for his great co-operation in printing my thesis. I am also thankful to my brother Ato Lulu Tsige and my friend Ato Hailemariam Ambaye who read part of the manuscript and my colleagues for their continued encouragement to complete this work.

CONTENTS

Abstract

Introduction 1

Chapter 1. II-VI Compound Semiconductors

1.1. Introduction 3

1.2. Self-compensation and deviation of Stoichiometry

in II-VI semiconductors 5

1.3. Electrical properties of II-VI compound materials 9

1.3.1. Electrical conductivity 9

1.3.1.1.- Intrinsic Conductivity 10

1.3.1.2.- Extrinsic Conductivity 13

Chapter 2. The Perturbed Angular Correlation (PAC) Technique

2.1. Introduction 16

2.2. Hyperfine interaction 18

2.3. Perturbed angular correlation (PAC) 22

2.3.1. Orientation of the EFG tensor 28

2.3.2. Probe atoms 30

2.3.3. The PAC spectrum 32

Chapter 3. Experimental Apparatus

3.1. Function of the PAC Apparatus 36

3.2. Components of the PAC Apparatus 40

Chapter 4. Thermodynamical investigation of the metal vacancy in ^{111}In Doped ZnSe

4.1. Motivation 51

4.2. Sample preparation 52

4.2.1. Introduction 52

4.2.2. Experimental Procedure 53

4.3. Results and Discussion 55

4.3.1. Temperature dependence of In-V pair concentration 58

4.3.2. Influence of the dopant In on the vacancy concentration 70

Conclusion **76**

Appendix **77**

References **79**

Abstract

Large scale application of the II-VI compound ZnSe has been hampered by the low conductivity of p-type ZnSe. Very recently, well-conducting p-type ZnSe samples have been produced, but it is still not known why acceptor doping of ZnSe is so difficult. Nonetheless, intrinsic point defects and impurities are blamed for this problem.

In the ZnSe semiconductor doped with In, the formation of In_{Zn} - V_{Zn} complexes is shown to occur using the radioactive dopant ^{111}In along with the perturbed $\gamma\gamma$ angular correlation technique which seem to be responsible for the self-compensation of In donors in ZnSe. The formation and dissociation of these complexes were observed following a rapid quench of the material during annealing between 300 and 700 K in vacuum. In light of this thermal stability of the complex, the migration energy of the metal vacancy defect V_{Zn} and its binding energy with the donor In is determined to be 1.30 ± 0.05 eV and 0.34 ± 0.03 eV respectively.

Introduction

ZnSe is a II-VI wide-band-gap compound semiconductor with a cubic zinc-blend structure. Its band gap of 2.7 eV is well suited for optical application specially for a blue semiconductor laser. Fabrication of ZnSe light-emitting diodes (LEDs) and laser requires the formation of p-n junction (or hetrojunctions) through controlled substitutional doping. Although p-type doping is currently the major obstacle to making such devices, efficient activation of n-type dopants in high concentrations is of equal importance, specially if ZnSe blue emitting lasers are to be developed.

However, little is known about the variety of intrinsic point defects in this material, mainly because their identification and their mutual interactions as well as their interactions with impurity atoms still pose a major problem [1]. Nevertheless, intrinsic point defects and impurities are blamed for the failure of making p-n junction devices out of wide-band-gap semiconductors in general and out of ZnSe in particular. The cause of this difficulty remains a puzzle and there is no firm evidence for any of the different explanations given to the problem. However, one of the oldest and most popular explanation suggests that the problem is related to compensation mechanisms in which dopant atoms lose their electrical activity due to the presence of compensating or passivating intrinsic defects or impurity atoms [1].

In order to investigate whether this problem is really connected to the generation of compensating native defects, atomistic information on these defects will be necessary to obtain a fundamental understanding of the doping mechanism involved. For this a wealth of experimental techniques is nowadays available. Among them, the nuclear techniques, such as the Perturbed $\gamma\gamma$ Angular Correlation technique (PAC) and the Mössbauer spectroscopy gather their information with the help of radioactive probe atoms introduced into the material of interest [2]. These techniques allow us to study the probe atom's environment on atomic scale, due to the hyperfine interaction of the electric and magnetic fields of the lattice with the nuclear moment of the probe atom.

In this paper, we use the PAC technique to study the thermodynamic behaviour of defects, such as metallic vacancies created due to a deviation from stoichiometry, in ZnSe crystal. Since the PAC technique exhibits a high microscopic sensitivity to changes of local structure within a few atomic distances, this method offers the possibility of detailed studies of different types of defects in our sample.

The first chapter reviews very shortly on the development of the study of II-VI wide-band-gap semiconductors and their electrical properties. In addition the role of native defects and deviations of stoichiometry in these semiconductors is considered.

The following two chapters discuss on the principles of the PAC technique and function of the PAC apparatus. The basic principle of PAC is that, by introducing a probe nucleus which decay by a $\gamma\gamma$ cascade, one is able to use the first gamma as a marker with which to correlate the angular dependence of the emission of the second gamma. By measuring the time dependence of the angular correlation, the strength of the hyperfine interaction between the quadrupole moment and the electric field gradient (EFG) experienced by a probe nucleus can be determined. These interactions can be used to label particular defects and relate them to material composition, structure and fabrication history.

The last chapter is devoted to sample preparation and discussion of the experimental results. By using the radioactive donor ^{111}In which at the same time is a probe atom for PAC, the formation of probe atom - defect complex is investigated. It is shown that the intrinsic lattice defect in ZnSe is the metal vacancy. Based on the formation and dissociation of the complex with temperature, the thermodynamic parameter that is migration energy of the metal vacancy and its binding energy with the donor In is determined. In addition, we discuss the behaviour of the metal vacancy concentration with respect to temperature and in relation to the decay of In. However, for a better understanding of the behaviour of vacancy concentration other measuring techniques are recommended.

CHAPTER ONE

II-VI Compound Semiconductors

1.1. Introduction.

Atoms from group IIb of the periodic table combine with atoms from group VIb to form crystalline semiconducting compounds. These semiconductors are called"***II-VI compounds***". They are not alloys but definite chemical compounds with a *1:1* atomic ratio between the II and VI atoms, which occupy alternate site in the crystal lattice.

II atoms have two valance electrons less, and VI atoms two electrons more than those atoms from group IV of the periodic table which form the elemental semiconductor diamond, germanium, silicon and gray thin. II-VI compounds have, therefore, the same average number of electrons per atom as the group IV semiconductors, and it is found that the compounds indeed have a crystal structure and electronic properties which are in many ways similar to those of the IV semiconductors. Nevertheless, II-VI compounds as a collective group of materials possesses characteristic properties that distinguish them from the group IV semiconductors [3]. These differences arise chiefly from the fact that the compound crystals have a lower symmetry than the group IV crystals and that, whereas the group IV semiconductors consist of covalently bound neutral atoms, the II-VI compounds contain positive and negative ions at the lattice sites.

The growth of semiconductor technology in the early 1950's highlighted the limitations of silicon and germanium of which perhaps the character and magnitude of the forbidden energy gap were the most disadvantageous. At first the extension in the range of energy gaps was sought in the III-V compounds, where considerable success has been achieved with InSb and GaAs in the low- and high- energy gap areas respectively. Concurrently with the latter developments in the III-V compounds,

systematic studies were made of several of the II-VI compounds. The results of these studies have revealed much about the general nature of the II-VI compounds and the feature of the chemical stability of the higher energy gap materials at room temperature offers an immediate advantage over the unstable III-V phosphides [3].

II-VI Compounds in their broadest sense include the oxides, sulphides, selenides and tellurides of beryllium, magnesium, zinc, cadmium and mercury. The general discussion in this paper will however centre around the sulphides, selenides and tellurides of zinc and cadmium and particularly on ZnSe. Direct gap seems to be a general character of the restricted range of II-VI compounds made above, and take one of two crystalline structures, zinc-blende and wurtizite, both of which are characterised by the tetrahedral lattice sites [3].

II-VI compounds on average have four valance electrons per atom; this is a situation conducive to the formation of tetrahedral lattice sites provided there is a tendency towards sharing rather than the transfer of electrons between them. These tetrahedra can be arranged into two forms of crystal structures: "***zinc-blende***" which is cubic, and " ***wurtizite***" which is hexagonal. The cubic zinc-blende structure is the same as the diamond form except that the two different kinds of atoms occupy alternate positions in the lattice. The wurtizite structure is similar to the zinc-blende except that alternate ⟨111⟩ layers are rotated through 180° about [111] axis, giving the structure hexagonal symmetry. The three compounds ZnS, CdS and CdSe have the wurtizite structure, whereas ZnSe, ZnTe and CdTe have the cubic zinc-blende structure.

The exploitation of the II-VI compounds for commercial purpose has occurred over the past fifty years. Wide-band-gap semiconductor with energy gaps in the visible region of spectrum, such as ZnSe, ZnS, CdS and ZnTe have potential technological applications, specially for optical devices using blue or green light, including semiconductor lasers and light emitting diodes. They are currently being used for efficient Tv phosphors and for thin film electroluiminescent displays [4].

Despite these remarkable achievements, the application of these materials in the p-n junction devices, however, has been hampered by the problems encountered in making both conducting n-type or p-type material. And the problem is ascribed to the so-called "***self-compensation***" in these materials due to the presence of native defects [5, 6].

1.2. Self-Compensation and deviation of stoichiometry in II-VI semiconductors.

Self-Compensation designates the phenomenon of impurity doping limitation due to native defects generated in the considered crystal. That is acceptors or donors introduced into a host material are compensated by inducing native defects, such as vacancies or interstitials. This phenomenon has been observed in a large number of wide-band-gap semiconductors and among them in several of the II-VI compounds: ZnS, ZnSe, CdS, CdSe, CdTe and ZnTe [7].

In the wide-band-gap semiconductors considered above the problem is particularly acute because typically one type of conduction (n-type or p-type) is very difficult to obtain and the expected technological applications are plagued by this major problem. For example, it is comparatively easy to make n-type ZnSe, but difficult to make p-type ZnSe. Detailed understanding of these phenomena has been lacking.

The most popular explanation of why it is hard to dope wide-band-gap semiconductors is the native defect compensation mechanism. In a II-VI compound semiconductor, the intrinsic lattice defects of importance are vacancies and host interstitials associated with each of the two sublattices. The larger chemical differences for the two constituents of a II-VI lattice make the presence of antisites, where atoms of one sublattice occupy sites on the other, less likely. According to the native defect mechanism, p-type ZnSe is compensated by native point defects that are donors.

The driving force for the formation of compensating defects would be the energy gained when electrons are transferred between the Fermi level and the electronic levels in the gap of the defects. For example, if acceptor dopants were used to place the Fermi

level in ZnSe near the valance band edge, then a native donor defect could recoup its formation energy by transferring an electron from its occupied electronic level near the conduction band edge to the Fermi level. The spontaneous formation of native defects would thus prevent the Fermi level from moving below a fixed value that is determined by the formation energies and electronic levels of the native defects, independent of the properties of the dopant that are used to fix the Fermi level and of how the material was prepared.

This self-compensation may be analyzed simply in terms of an energy balance equation, i.e., energy must be supplied by the crystal to produce the 'excess' concentration of defect centres while energy is gained by the crystal by the interaction of the defects with the free carriers produced by the added impurity centres. Clearly, if the energy of defect formation is large compared to the energy gained by compensation, very little self-compensation will take place. On the other hand, if the energy of defect formation is small compared to the energy gained by compensation, all free carriers will be compensated by the formation of defects and only insulating crystals will be accessible by equilibrium processes [8].

The energy gained by this compensation would be of the order of the band-gap energy (fig. 1), so that the tendency to native defect compensation would increase as the band gap increases [9,10].

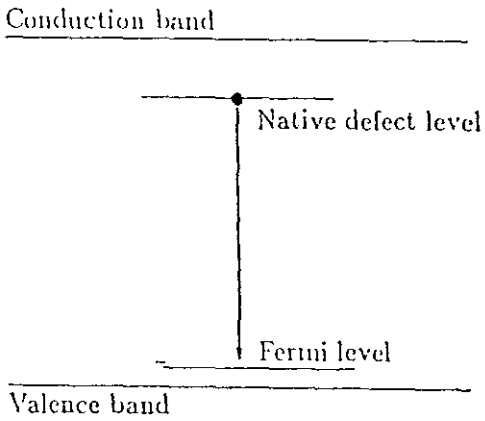

Fig. 1. *Native defect compensation in p-type ZnSe [9].*

Fig. 1 shows native defect compensation in p-type ZnSe. According to the native defect mechanism, native donor defects are formed when ZnSe is doped p-type. These defects gain back much of their energy of formation by transferring electrons from defect levels near the conduction band to the Fermi level near the valance band. The energy gain due to electron transfer can be of the order of the band gap energy.

The prevention of the Fermi level from moving below a fixed value by native defects would explain why doping problems occur in all wide-band-gap materials, and are less severe in medium-gap materials such as CdTe (which can be doped n and p type). It would also explain why the difficulty in producing p-type (or n-type) material is universal, appearing for all growth and doping techniques and for all dopants. That these materials can be doped n-type and not p-type, or vice versa, can be explained if the native defects with the lowest formation energy are donors in some materials and acceptors in others. For example, Jansen and Sankey have suggested that the native defect mechanism can account for the difference between ZnSe, which can be made n-type, and ZnTe, which can be made p-type, even though the two materials are strikingly similar in other ways [11].

The native defect mechanism thus gained wide popularity because it provided a simple explanation of why doping problems are endemic to almost all wide-band-gap semiconductors. There is, however, no direct evidence to either confirm or deny the role of native defects in wide-band-gap semiconductors.

The II-VI compounds of Zn, Cd, S, and Se have direct band gaps ranging from 1.84 to 3.91 eV at low temperature. They readily form mixed crystals and thus have the capability of generating efficient luminescence through out the visible spectrum. Unfortunately, these materials have never been made low-resistivity p-type, despite studies in numerous industrial laboratories [12].

A great deal of effort has been made to fabricate both p- and n-type materials of ZnSe, which is a typical wide-band-gap semiconductor with an energy gap of 2.8 eV,

since ZnSe is expected to be a useful material for optoelectronic devices. The technique for control of n-type doping for ZnSe has been well established. However, there have been difficulties in producing highly conductive p-type ZnSe, and it has been regarded as due to the self-compensation effect. Recently, this difficulty appears to have been surmounted; in fact, Haase et al. [13] have succeeded in demonstrating a ZnSe semiconductor diode. Their success made the occurrence of self-compensation in p-type ZnSe questionable. The doping was achieved during molecular beam epitaxy growth of ZnSe by introducing a substitutional nitrogen acceptors. Net acceptor concentrations as high as 10^{18} /cm^3 have been obtained in this way [14,15].

However, the actual N concentration in the samples is found to be 3-5 times larger than the acceptor concentration, suggesting that under high N incorporation rates, self- compensation becomes very important.

Despite these impressive recent experimental advances, the cause of the doping problem has remained unclear and it is still unknown why acceptor doping of ZnSe is so difficult. Several explanations for the difficulty have been considered: (1) Self-compensation by native defects is one possibility, but this mechanism would predict the impossibility of p-type doping regardless of dopant, which seems inconsistent with the success of p-type doping of ZnSe using N. The native defect compensation may be due to deviations from stoichiometry; (2) Self-compensation by the dopant when a substitutional acceptor becomes a donor by moving to an interestitial site; and (3) the solubility of the dopants.

Theoretical results show clearly that the native defect concentrations in stoichiometric ZnSe are too low to be a significant source of compensation, whereas undetectably small deviations from stoichiometry can produce large concentrations of native defects. It has been found that the defects formed depend on whether the sample is n-type or p-type, but always compensate. Hence deviations from stoichiometry can not explain why ZnSe can be doped n-type but not p-type, because they are as likely to compensate n-type material as p-type [16]. Having eliminated native defects as the

source of doping problems in ZnSe it is important to identify the microscopic origin of the difficulty.

1.3. Electrical properties of II-VI compound materials.

Of fundamental importance to the electronic properties of a material is the presence of defects. Solid-state electronics relies on the possibility of altering the electric properties of intrinsic semiconductors via doping with chemical impurities. Changes in electrical properties due to the introduction of defects arise from either changes in the number or in the mobility of the current carriers or both.

Most of the electronic and optical properties of semiconductors are determined by electrically active defects (intrinsic defects or impurities). Even small concentrations (10^{-6} or less) may have a strong influence, and important parameters like conductivity or carrier life time can be varied within orders of magnitude by doping the semiconductor with appropriate impurities. The basic property of these defects is the existence of a localized electronic state with an energy level in the band gap [17]. The defect concentrations will depend on factors such as stoichiometry, temperature, chemical potential, and the presence of extrinsic impurities. Impurity-atom sites in the host are classed as substitutional and interestial and both types alter the electrical characteristics of the impure or doped material. Of primary importance in doped materials are impurities from groups adjacent to the host material in the periodic table, groups I, III, V and VII for II-VI compound semiconductors, which substitutionally enter the host semiconductor crystal lattice. These impurities are expected to produce shallow levels in the band-gap, donor levels for group III and VII and acceptor levels for group I and V elements.

1.3.1. Electrical conductivity

The general expression for conductivity σ in a semiconductor is the sum of the electron and hole contributions and is given by

$$\sigma = e(n\mu_n + p\mu_p) \tag{1.1}$$

where μ_n and μ_p are the electron and hole mobilities respectively and mobility is defined to be the magnitude of the drift velocity per unit electric field. The carrier concentrations n and p are dependent upon the location of the Fermi energy E_F and can be represented in a simple form for intrinsic semiconductors at most temperatures and for extrinsic semiconduction at low temperatures. Expressions for these particular cases assuming parabolic energy bands are given below.

1.3.1.1. Intrinsic Conductivity

A pure, single-crystal semiconductor, in which all the electrons in the conduction band have been thermally excited from the valance band, is called an intrinsic semiconductor.

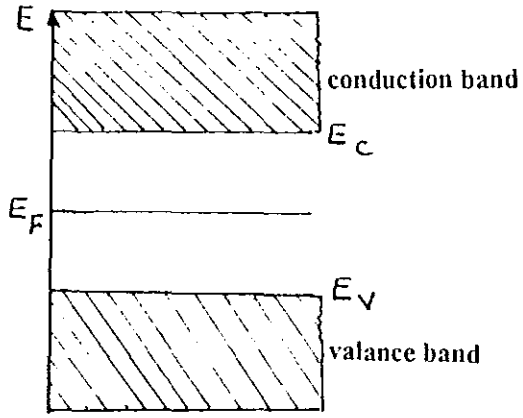

Fig. 2. *Simplified band diagram for an intrinsic semiconductor.*

To find the concentration of intrinsic carriers in terms of the band gap, the Fermi-Dirac distribution function must be employed with the assumption of parabolic band edges. This function f(E):

$$f(E) = \frac{1}{1+\exp\frac{E-E_F}{k_B T}} \tag{1.2}$$

gives the probability that a level of energy E is occupied. At the temperatures of interest we may suppose for the conduction band of a semiconductor that $E-E_F >> kT$ and the Fermi-Dirac distribution function reduces to

$$f \approx \exp \frac{E_F - E_c}{k_B T} \tag{1.3}$$

The energy of an electron in the conduction band is

$$E_k = E_c + \frac{h^2 k^2}{8\pi^2 m_e} \tag{1.4}$$

Where E_c is the energy at the conduction band edge as in fig.(2), k is the value of the wave-vector $\vec{K}$ at the bottom of the conduction band and m_e is the effective mass of an electron. Thus the density of states at E is [18].

$$D_e(E) = \frac{1}{2\pi^2}\left(\frac{8\pi^2 m_e}{h^2}\right)^{3/2}(E - E_c)^{1/2} \tag{1.5}$$

The concentration of electrons in the conduction band is

$$n = \int_{E_C}^{\infty} D_e(E) f_e(E) dE \tag{1.6}$$

On substituting equations (1.3) and (1.5) into this expression and integrating, we obtain

$$n = 2\left[\frac{2\pi m_e k_B T}{h^2}\right]^{3/2} \exp\left(\frac{E_F - E_c}{k_B T}\right) \tag{1.7}$$

The problem is solved for n when E_F is known. Similar consideration for the calculation of the equilibrium concentration of holes p in the valance band results:

$$p = 2\left[\frac{2\pi m_h k_B T}{h^2}\right]^{3/2} \exp\left(\frac{E_v - E_F}{k_B T}\right) \tag{1.8}$$

We multiply together the expression for n and p to obtain the equilibrium relation, with the energy gap $E_g = E_c - E_v$,

$$np = 4\left(\frac{2\pi k_B T}{h^2}\right)^3 (m_e m_h)^{3/2} \exp\left(\frac{-E_g}{k_B T}\right) \tag{1.9}$$

Since in an intrinsic semiconductor the number of electrons is equal to the number of holes, it is then possible to determine the temperature dependence of intrinsic concentrations n_i . Thus, from (1.9) we have,

$$n_i = 2\left(\frac{2\pi k_B T}{h^2}\right)^{3/2} (m_e m_h)^{3/4} \exp\left(\frac{-E_g}{2k_B T}\right) \tag{1.10}$$

The intrinsic carrier depends exponentially on $E_g /2k_B T$ where E_g is the energy gap, since the three-halves power term in T, and any power term in the mobility, is swamped by the exponentially temperature dependent term. Then the conductivity becomes

$$\sigma = e n_i (\mu_n + \mu_p)$$

$$= e(\mu_n + \mu_p) 2\left(\frac{2\pi k_B T}{h^2}\right)^{3/2} (m_e m_h)^{3/4} \exp\left(\frac{-E_g}{2k_B T}\right) \tag{1.11}$$

$$= \sigma_{oi} \exp\left(\frac{-E_g}{2k_B T}\right)$$

where,

$$\sigma_{oi} = e(\mu_n + \mu_p) 2\left(\frac{2\pi k_B T}{h}\right)^{3/2} (m_e m_h)^{3/4} \tag{1.12}$$

The temperature dependence of conductivity is dominated by the exponential dependence of carrier concentration. However, the scope of electrical measurement is limited to impure materials and in any event there is really no II-VI compound, in which there is any hope of observing intrinsic conductivity at room temperature [3].

1.3.1.2. Extrinsic Conductivity

Semiconductors whose electrical properties are dominated by impurities are called extrinsic semiconductors. These are the materials most often used in device fabrication. In the extrinsic range, while the carrier concentration in the bands is still determined by (1.7) and (1.8), the position of the Fermi level is determined by the impurity centres, so that in order to determine the carrier concentration the relation between the position of the Fermi level and that of the impurity centres must be discussed. Consider first a system in which a concentration N_d of donor impurities is present, each being able to contribute one electron to the system [19,20,21].

Consider the case shown in fig.(3), where donor impurities with the concentration N_d and with energy level E_i are added to the crystal. At low temperature

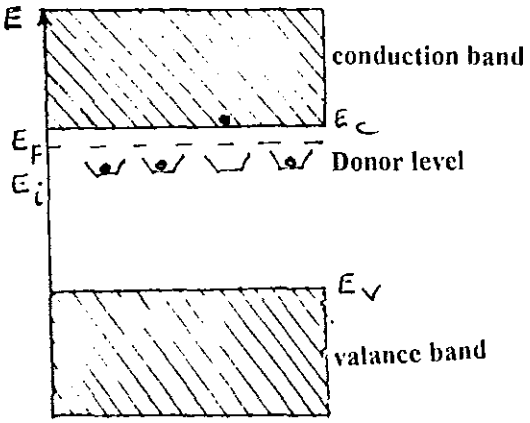

Fig. 3. *Energy diagram of a semiconductor containing a donor level located at energy* E_i

the concentration of electrons in theconduction must equal to the concentration of ionized donors, or for the present case,

$$n_c = N_d\left(1 - \frac{1}{\exp\frac{E_i - E_F}{k_B T} + 1}\right) \tag{1.13}$$

and for low temperature case, $E_F - E_i >> k_BT$

$$n_c \approx N_d \exp\left(\frac{E_i - E_F}{k_B T}\right) \tag{1.14}$$

On using equation (1.7), this can be written as

$$2\left[\frac{2\pi k_B T m_e}{h^2}\right]^{3/2} \exp\left(\frac{E_F - E_c}{k_B T}\right) = N_d \exp\left(\frac{E_i - E_F}{k_B T}\right) \tag{1.15}$$

From this the Fermi level can be uniquely determined as

$$E_F = \frac{E_c + E_i}{2} + \frac{k_B T}{2} \ln\left(\frac{N_d}{2\left(\frac{2\pi k_B T m_e}{h^2}\right)^{3/2}}\right) \tag{1.16}$$

The approximate expression for the electron concentration is then,

$$n_c = \sqrt{2N_d}\left[\frac{2\pi k_B T m_e}{h^2}\right]^{3/4} \exp\left(\frac{-E_d}{2k_B T}\right) \tag{1.17}$$

where, $E_d = E_c - E_i$. Identical results hold for acceptors, under the assumption of no donor atoms.

Then the total conductivity of our material will be

$$\sigma = \sigma_i + \sigma_e \tag{1.18}$$

$$\sigma = \sigma_{oi} \exp\left(\frac{-E_g}{2k_B T}\right) + \sigma_{oe} \exp\left(\frac{-E_d}{2k_B T}\right) \tag{1.19}$$

Where, $\sigma_{oe} = e\mu_n \sqrt{2N_d}\left[\frac{2\pi k_B T m_e}{h^2}\right]$

Unfortunately, the II-VI compound semiconductors, because of the ionic character in the bond type, exhibits compensation effects for either impurity type with the

result that high resistivities tend to prevail [3]. On top of that the above discussion assumes the conductivity to be isotropic and is open to criticism particularly in respect of the anisotropy of the wurtzite structured materials. These materials require a tensor to describe the conductivity and as such is beyond the scope of this paper.

Since it is extremely difficult to prepare II-VI material containing one type of impurity, the value of n_c in simple terms is more likely to be given by

$$n_c = N_d - N_a \qquad \text{(Assuming } N_a < N_d\text{)} \qquad (1.20)$$

Such material is usually described as "*compensated*" since the available number of conduction electrons is less than the number of impurity centres.

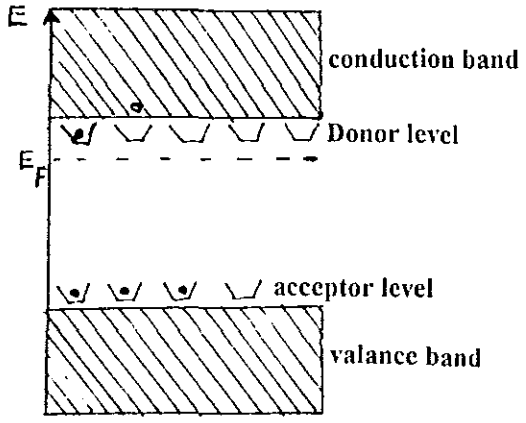

Fig. 4. *Energy diagram of compensated semiconductor.*

Many electrical and optical methods are available to detect the capture and emission of charge carriers by impurity levels and to measure their rates. All of these methods are working in nonequilibrium conditions; in many cases, a macroscopic transport property (e.g. current and capacitance) is measured which is indirectly sensitive to the impurity transitions via their influence on the electron distribution in the bands. The perturbed angular correlation (PAC) spectroscopy, however, is sensitive to the charge distribution around a probe atom on an atomic scale. If such a probe atom is part of an electrically active complex, the charge transition can be observed directly. In this sense, the technique is strictly complementary to classical methods.

CHAPTER TWO

The Perturbed Angular Correlation (PAC) Technique

2.1. Introduction

The PAC technique is sensitive to hyperfine interactions in excited nuclear states. Basically, it is not an energy measurement but rather a phase-sensitive method and for that reason no information about the ground-state splitting is obtained [22]. It was originally developed and applied to the determination of magnetic dipole and electric quadrupole moments of excited nuclear states, a domain of nuclear physicists. The possibility to get information about internal magnetic fields or electric field gradients, which interact via a hyperfine interaction with the nuclear moments, opened up the field to solid state physics.

The hyperfine interaction between a nuclear moment - magnetic dipole or electric quadrupole - and electromagnetic fields lifts the degeneracy of the M states of a nuclear level with spin I (fig.5) for the case of a quadrupolar interaction. For measuring the accompanying energy differences ΔE that characterize the induced level splitting in a unique way a wealth of experimental techniques have been developed. Among them are techniques making use of a resonance effect, e.g., Mössbauer spectroscopy and the different, highly sophisticated varieties of ESR and NMR; they all measure directly the energy ΔE. Other techniques like PAC or μSR operate in the "***time domain***" rather than in the "***energy domain***" and measure the precession frequency ω of the nuclear spins, which is related to the energy difference by $\omega = 2\pi\left(\frac{\Delta E}{h}\right)$. These techniques make use of the coupling between the emission probability of a particular type of radiation in space and the actual direction of the nuclear spin I.

For stable nuclei, the neutron and proton numbers are favourable for stability. For unstable nuclei the neutron and proton numbers are not favourable for stability and this

relative number tries to reach a correct stability ratio by undergoing radioactive decay of the nucleus. Three kinds of radiations can accompany radioactive decay of the nucleus. These are alpha rays, beta rays and gamma rays. Of course, gamma decay does not change the neutron to proton ratio.

From nuclear spectroscopy it is known that angular correlation may exist between nuclear (α, β, γ) radiation emitted from unstable nuclei. The basic idea of angular correlation stems from the fact that the probability of photon emission from a radioactive nucleus depends, in general, on the angle between the nuclear spin axis and the direction of emission. From the observed correlations nuclear properties like spin angular moment I, can be determined. However, the angular correlations may be perturbed by interactions occurring between the decaying nuclei and their chemical environment. From these perturbations, information about the electronic configuration or the crystal structure can be obtained.

Perturbed $\gamma\gamma$ Angular Correlation (PAC) technique gathers its information with the help of radioactive probe atoms introduced into the material of interest. This technique allows us to study the probe atom's environment on an atomic scale due to the hyperfine interaction of the electric and magnetic fields of the lattice with the nuclear moment of the probe atom. Thus, we can get fundamental understanding of the involved doping mechanism [23,24,25,26].

The PAC technique has successfully made use of the electric field gradient (EFG) for the study of defects primarily in metals and stimulating results in metals established PAC as a powerful new tool for the investigation of defects in semiconductors [2].

Using PAC, full information concerning the number of different fields and their strengths, acting on probe atoms, is transmitted by the frequency modulated radiation field. The information obtained in that way is microscopic and local in its nature, since the field strength decreases rapidly with increasing distance from the probe atom.

Therefore, mainly contributions originating from the first shell of surrounding lattice atoms are observed [27].

2.2. Hyperfine interaction

The hyperfine interaction arising from the interaction of an electromagnetic field with a nuclear moment, magnetic dipole or electric quadrupole, which is observed in PAC experiments allows the detection of magnetic or electric fields that are present at the site of the nucleus [28].

Defects, such as intrinsic lattice defects or impurity atoms, create a typical electric field gradient (EFG) at the site of the neighbouring lattice atoms. This EFG is determined via its interaction with the nuclear electric quadrupole moment of a radioactive probe atom. The interaction between the nuclear electric charge distribution and the charge distribution of the surrounding electrons and positive ions results in an energy shift of nuclear states. The magnitude of this energy is

$$E_{el} = \int \rho(\vec{r})\Phi(\vec{r})d^3r \tag{2.1}$$

where $\rho(\vec{r})$ is the charge density inside the nucleus and $\Phi(\vec{r})$ is the potential at the site of the nucleus produced by the surrounding electric charge distribution. Through Taylor expansion of $\Phi(\vec{r})|_0$, we will obtain an elegant physical interpretation of E_{el} i.e.

$$\Phi(\vec{r}) = \Phi_o + \sum_{i=1}^{3}\left(\frac{\partial\Phi}{\partial x_i}\right)_o \cdot x_i + \frac{1}{2}\sum_{ij}\left(\frac{\partial^2\Phi}{\partial x_i\partial x_j}\right)_o \cdot x_i x_j + \ldots \tag{2.2}$$

putting this in the expression above, the electrical energy E_{el} becomes

$$E_{el} = \Phi_o\int\rho(\vec{r})d^3r + \sum_{i=1}^{3}\left(\frac{\partial\Phi}{\partial x_i}\right)_o\int\rho(\vec{r})x_i d^3r + \frac{1}{2}\sum_{ij}\left(\frac{\partial^2\Phi}{\partial x_i\partial x_j}\right)_o\int\rho(\vec{r})x_i x_j d^3r + \ldots \tag{2.3}$$

$$= E_o + E_1 + E_2 + \ldots$$

Where E_0, E_1 and E_2 represent monopole, dipole and quadrupole terms of E_{el} respectively. The monopole term E_0 represents the coulomb energy of the surrounding charge distribution on the nucleus and its contribution is to the potential energy of the crystal lattice. The dipole term E_1 represents dipole interaction of the electric field $\vec{E} = -\vec{\nabla}\phi$ with the nuclear dipole moment. But, due to the definition of parity for a nucleus, the nuclear dipole moment vanishes. Also terms higher than the third term are negligible because of their too small interaction energies. Thus, the only term which is interesting to us is E_2. In order to obtain the expression for the quadrupole term, E_2 will be written as

$$E_2 = \frac{1}{2}\sum_{i,j}\left(\frac{\partial^2\Phi}{\partial x_i \partial x_j}\right)_o \int \rho(\vec{r}) \cdot x_i x_j d^3r$$

$$= \frac{1}{6}\sum_{i,j}\left(\left(\frac{\partial^2\Phi}{\partial x_i \partial x_j}\right)_0 - \frac{1}{3}Tr\underline{\underline{\Phi}} \cdot \delta_{ij} + \frac{1}{3}Tr\underline{\underline{\Phi}} \cdot \delta_{ij}\right)\int \rho(\vec{r}) \cdot \left(3x_i x_j - r^2\delta_{ij} + r^2\delta_{ij}\right) d^3r$$

$$= \frac{1}{6}\sum_{i,j}\left(\frac{\partial^2\Phi}{\partial x_i \partial x_j}\right)_o \int \rho(\vec{r}) \cdot \left(3x_i x_j - r^2\delta_{ij}\right) d^3r - \frac{1}{18}Tr\underline{\underline{\Phi}}\sum_i \int \rho(\vec{r}) \cdot \left(3x_i^2 - r^2\right) d^3r$$

$$+\frac{1}{6}\int \rho(\vec{r}) \cdot r^2 d^3r \sum_i \left(\left(\frac{\partial^2\Phi}{\partial x_i^2}\right)_0 - \frac{1}{3}Tr\underline{\underline{\Phi}}\right) + \frac{1}{18}Tr\underline{\underline{\Phi}}\sum_i \rho(\vec{r}) \cdot \left(3x_i^2 - r^2\right) d^3r$$

$$+\frac{1}{6}Tr\underline{\underline{\Phi}}\int \rho(\vec{r}) \cdot r^2 d^3r \qquad (2.4)$$

where, $Tr\underline{\underline{\Phi}} = \sum_i \Phi_{ii}$

Finally we get

$$E_2 = \frac{1}{6}\sum_{i,j}\left(\frac{\partial^2\Phi}{\partial x_i \partial x_j}\right)_0 \int \rho(\vec{r}) \cdot \left(3x_i x_j - r^2\delta_{ij}\right) d^3r + \frac{1}{6}Tr\underline{\underline{\Phi}}\int \rho(\vec{r}) \cdot r^2 d^3r \qquad (2.5)$$

The first term (quadrupole term) in the expression of E_2 can be shown to be caused by the interaction of the nuclear electric quadrupole moment Q with the 3x3 tensor of the electric field gradient (EFG) V_{ij}, which is the second derivative of the

electrostatic potential V at the site of the nucleus (r=0) [29]. The quadrupole interaction can then be described by [27].

$$E_Q = \frac{e \cdot Q \cdot V_{zz}}{4I(2I-1)}\left(3I_z^2 - I(I+1) + \frac{\eta}{2}\left(I_+^2 + I_-^2\right)\right) \tag{2.6}$$

where I_z, I_+ *and* I_- designate angular momentum operators.

Two components are sufficient to completely describe the EFG since it is traceless. Usually chosen are the largest component V_{zz}, measuring the "***strength***" of the EFG, and the asymmetry parameter η which is defined as

$$\eta = \frac{(V_{xx} - V_{yy})}{V_{zz}} \tag{2.7}$$

with the convention $|V_{xx}| \leq |V_{yy}| \leq |V_{zz}|$ so that $0 \leq \eta \leq 1$ holds. It reflects the deviation of the EFG tensor from axial symmetry case i.e., $V_{xx} = V_{yy}$. The symmetry of the EFG corresponds directly to the symmetry of the probe's environment. The remaining three parameters necessary to describe the tensor within an arbitrary chosen system of coordinates, e.g., the coordinates of the host crystal, correspond to the three Euler angles that describe the transformation of the principal - axis system [28].

The energy shift $E_Q(M)$ of a nuclear state with spin I and Z component M that is caused by an axially symmetric field gradient ($\eta = 0$) is given by

$$E_Q(M) = \left[3M^2 - I(I+1)\right]\frac{e \cdot Q \cdot V_{zz}}{4I(2I-1)} \tag{2.8}$$

Detailed mathematical explanation is given in the Diploma work of Uwe Ott [29]. And the energy difference between two different sublevels M and M` of the same I is

$$\Delta E = E_Q(M) - E_Q(M') = \frac{3}{2\pi}\left(M^2 - M'^2\right)\hbar\omega_Q \tag{2.9}$$

with the transition frequency

$$\omega_Q = \frac{\pi \cdot e \cdot Q \cdot V_{zz}}{2I(2I-1)\hbar} \tag{2.10}$$

The smallest observable spin precession frequency is

$$\omega_0 = 3\omega_Q \text{ for I integer and,}$$

$$\omega_0 = 6\omega_Q \text{ for I half odd integer} \tag{2.11}$$

and the other observable frequencies are integer multiples of ω_o. The strength of the electric quadrupole interaction is defined by the spin independent product

$$\nu_Q = \frac{e \cdot Q \cdot V_{zz}}{h} \tag{2.12}$$

known as nuclear quadrupole coupling constant.

For a spin I = 5/2 the frequencies are:

$$\omega_1 = 2\pi \frac{(E_Q(\pm 3/2) - E_Q(\pm 1/2))}{\hbar} = \frac{6\pi}{20} e \cdot Q \cdot \frac{V_{zz}}{\hbar} = \omega_o$$

$$\omega_2 = 2\pi \frac{(E_Q(\pm 5/2) - E_Q(\pm 3/2))}{\hbar} = \frac{12\pi}{20} e \cdot Q \cdot \frac{V_{zz}}{\hbar} = 2\omega_o \tag{2.13}$$

$$\omega_3 = \omega_1 + \omega_2 = \frac{18\pi}{20} e \cdot Q \cdot \frac{V_{zz}}{\hbar} = 3\omega_o$$

In the case of nonaxially symmetric electric field gradient, i.e., $\eta > 0$, equation (2.6) has to be diagonalized for each η because the angular momentum operators $I_+ = I_x + iI_y$ and $I_- = I_x - iI_y$ mediate transitions between the different M states. For the nuclear spin I = 5/2, fig.(5) shows the energy shift E_M for the three sublevels M as a function of the asymmetry parameter η.

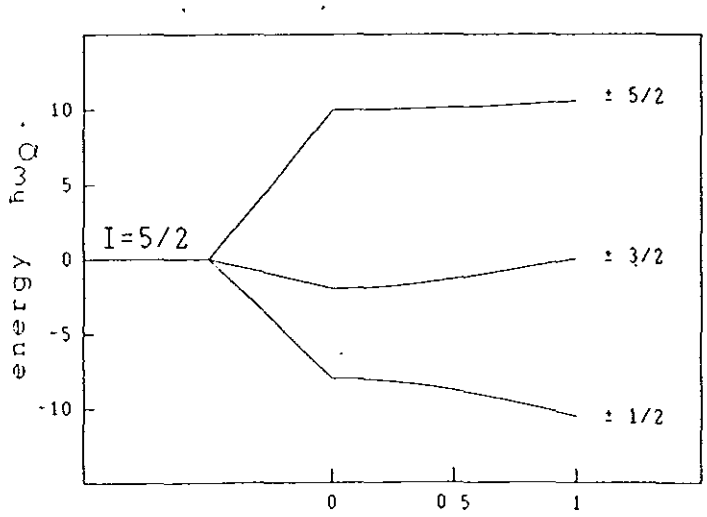

Fig. 5. *Level splitting of a nuclear state caused by an electric field gradient with asymmetry parameter η [28].*

2.3. Perturbed γγ Angular Correlation (PAC)

The basic principle of PAC is that a radioactive probe atom creates through its β decay an excited daughter nucleus which subsequently releases its excitation energy through the emission of two γ-rays. It is the property of the γ-rays to carry their angular momentum either along or opposite to their propagation direction which gives the information on the orientation of the nuclear spin I. By detecting both γ-rays, γ_1 and γ_2 (emitted from the same nucleus), in coincidence, information is obtained on the two orientations of the same nuclear spin I at the time of the emission of the γ-rays. And a change in the nuclear spin orientation I of the probe atom during the time interval between the emission of the γ -rays addresses the presence of defects and the precessional frequency ω is proportional to the strength of the field at the site of the nucleus. The spin precession is due to the hyperfine interaction between the nuclear moment of the probe atom and an extra nuclear field. Thus, whenever a radioactive probe atom decays, information about the field strength at its lattice site is delivered to the experimentalist via this frequency ω.

The phenomenon of conservation of angular momentum and the angular distribution of electromagnetic radiation with respect to its angular momentum vector l helps to get an understanding of how the orientation of a nuclear spin **I** can be monitored via the detection of the emitted γ-radiation. For a photon with angular momentum l=1, the two angular distributions are shown in fig.(6).

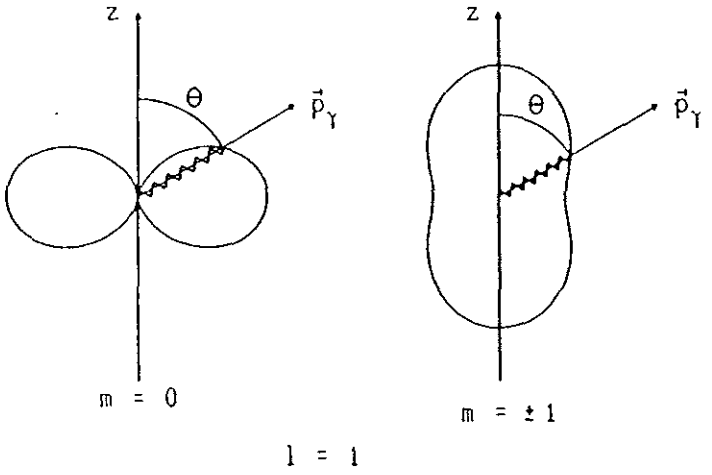

Fig. 6. *Angular distribution of γ-radiation with angular momentum l [28].*

The two different angular distributions, 1/2 $\sin^2\theta$ for m = 0 and 1/4 $(1+\cos^2\theta)$ for m =±1, describes the probability of observing the radiation along the direction P_γ enclosing an angle θ with the quantization axis z. The distribution shows that the probability to find a photon in z - direction is zero for m = 0, i.e., l is perpendicular to the flight direction. This relationship between the direction of l and the flight direction P_γ of a photon can now supply information about the orientation of the nuclear spin I, because of conservation of angular momentum. Of course, the superposition of the three m states, i.e., averaging over all m states, would result in an isotropic distribution; that means, for all angle θ the same γ intensity would be observed.

Let us consider a nucleus in an excited nuclear state E_i which decays to a lower lying level E_f via an intermediate state emitting two consecutive γ rays γ_1 and γ_2 with energies $E_{\gamma 1} = E_i - E$ and $E_{\gamma 2} = E - E_f$ (fig.(7)), both of which possess l=1 according

to the chosen 0-1-0 sequence of the nuclear spins I_i, I and I_f respectively.

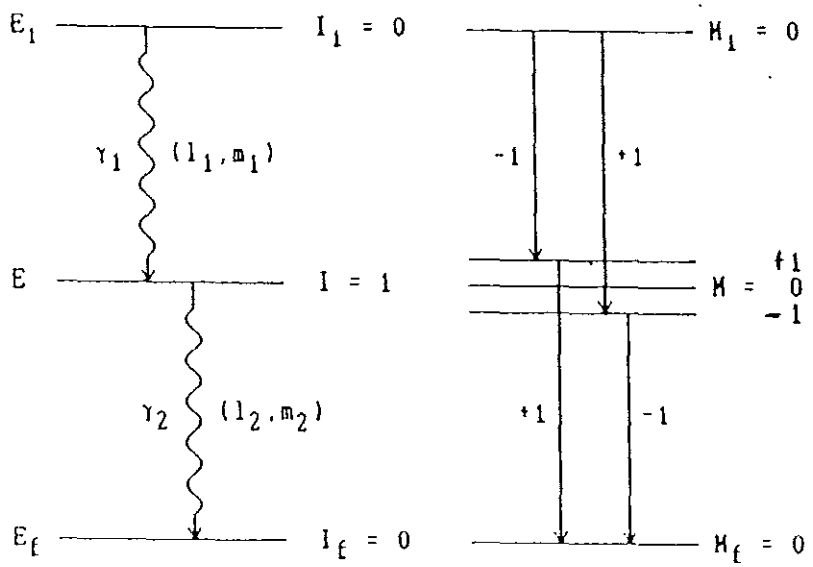

Fig. 7. *Nuclear decay scheme with the relevant parameter of a γγ cascade [28].*

The different energies $E_{\gamma 1}$ and $E_{\gamma 2}$ will be used to distinguish between the detection of γ_1 and γ_2 by using detectors which are at a relative angle θ_0 to each other as shown in fig.(8).

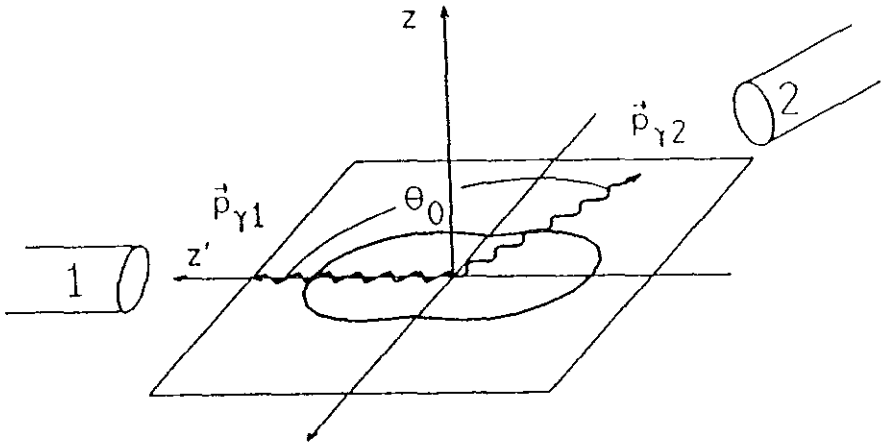

Fig. 8. *Experimental arrangement for detecting a γγ angular correlation [28].*

Choosing the momentum direction $P_{\gamma 1}$ of the photon as quantization axis, only photon states with $m_1 = \pm 1$ are possible. Consequently, the nucleus in its intermediate

state (**I** = 1) can only be in the state M = -1 or +1 because of the conservation of angular momentum. i.e.,

$$I_i = I + l_1 \tag{2.14}$$

for the corresponding projections we have [30].

$$M + m_1 = M_i \tag{2.15}$$

Whereas the state M = 0 can not be populated by this transition. That means, by detecting γ_1 we produce an alignment of the nuclear spins **I** with regard to $P_{\gamma 1}$, whereby in the present case all spins are pointing along $P_{\gamma 1}$.

For the second γ-transition, γ_2, we have again $l_2 = 1$ since it connects the nuclear states with spin **I**=1 and $\mathbf{I}_f$ =0, and if it is recorded in coincidence with γ_1 then $m_2 = \pm 1$ since the sublevel M = 0 is not populated. Note that recording of γ_2 without the coincidence condition would result in an isotropic distribution because also the state m_2 = 0 of γ_2 would contribute in this case. However, because of the preceding detection of γ_1 the probability W(θ) to detect γ_2 at an angle θ with respect to $P_{\gamma 1}$ and in coincidence with γ_1 becomes anisotropic and depends on the angle θ.

$$W(\theta) = \tfrac{1}{2}(1 + \cos^2\theta) \tag{2.16}$$

This angular correlation can be used for measuring the precession frequency of I caused by an extra nuclear magnetic or electric field: by detecting γ_1 a start time (t = 0) is defined and the initial spin alignment is known. By detecting γ_2 the stop time and thereby the elapsed time interval is known and any possible change of the nuclear spin alignment becomes observable via an altered angular correlation W(θ). The rotation of the aligned spins **I** through an angle ωt about the z-axis corresponds to a rotation of the reference frame through the same angle in the opposite direction so that θ_0 becomes θ_0 - ωt and the angular correlation becomes

$$G_{kk}(t) = S_{ko} + \sum_{n=1}^{3} S_{kn}\cos(\omega_n t) \tag{2.20}$$

and $\omega_1 + \omega_2 = \omega_3$. Where the frequencies ω_n contain information on the strength (V_{zz}) and, along with the amplitudes S_{kn}, on the asymmetry (η) of the electric field gradient tensor. The angular correlation function for the most often used probe atom for PAC experiment, ^{111}In, can be obtained with the help of angular correlation coefficients. These coefficients are [29].

$$A_{oo} = 1$$

$$A_{22} = -0.183$$

$$A_{24} = -0.212$$

$$A_{42} = -0.001$$

$$A_{44} = -0.002$$

A_{44} and A_{42} can be neglected since they are very small. A_{24} in polycrystalline case does not exist, and for a polycrystalline probe only the coefficients A_{00} and A_{22} contributes to the angular correlation function. Then the angular correlation function simplifies to:

$$\begin{aligned} W(\theta, t) &= 1 + A_{22}G_{22}(t)P_2(\cos\theta) \\ &= 1 + A_{22}\left(S_{20} + \sum_{n=1}^{3} S_{2n}\cos(\omega_n t)\right)\cdot P_2(\cos\theta) \end{aligned} \tag{2.21}$$

The strength of V_{zz}, the largest component of the EFG tensor, can be obtained from the smallest interaction frequency ω_1.

$$\omega_1 = g(\eta)\left(\frac{3\pi}{10}\right)\frac{e\cdot Q\cdot V_{zz}}{h} = g(\eta)\frac{3\pi}{10}\nu_Q \tag{2.22}$$

and the asymmetry parameter $\eta = (V_{xx} - V_{yy})/V_z$ describing the symmetry of the EFG tensor, is obtained from the frequency ratio ω_2/ω_1, which varies between 2 and 1 for $0 \le \eta \le 1$; at the same time, the factor g increases from 1 to 1.763 (fig. 9). For an axially

symmetric tensor (i.e., $\eta = 0$), $g = 1$ and the three frequencies are integer multiples of the fundamental frequency ω_1, i.e., $\omega_n = n\omega_1$.

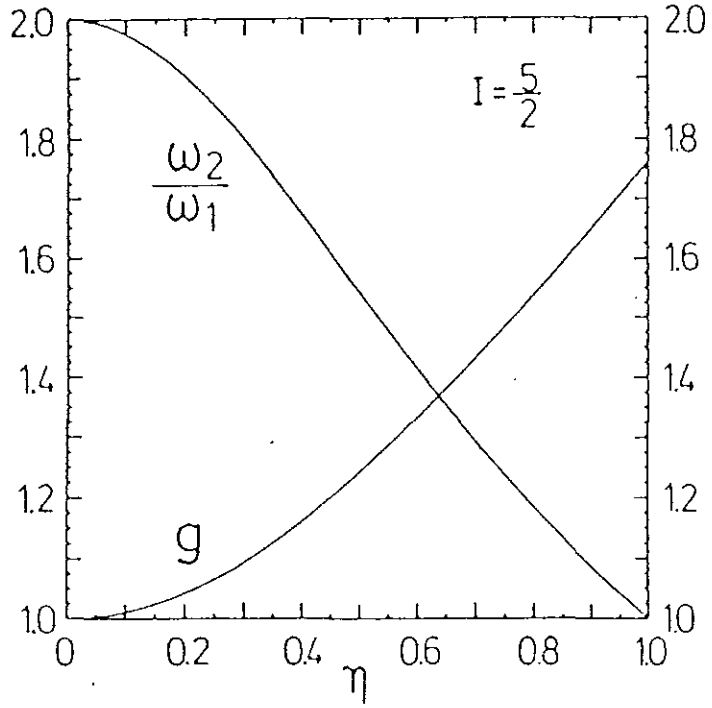

Fig. 9. *Dependence of the frequencies* ω_2/ω_1 *and of the parameter* $g(\eta)$ *on the asymmetry parameter* η *for the probe atom* ^{111}In *[2].*

2.3.1. Orientation of the EFG tensor.

The orientation of the field and its symmetry are important parameters which determine the final form of the perturbation factor $G_{kk}(t)$ since, in general, S_n depends on the direction along which the γ-rays are detected with respect to the principal axis system of the EFG tensor; the frequencies ω_n are not affected. Since a particular probe atom - defect complex possesses a particular crystallographic orientation also it's EFG tensor has a preferred orientation and therefore influences the measured S_n amplitudes in a characteristic way.

For practical reasons the principal axis system of the EFG tensor is described with reference to the lattice of the host crystal and therefore also the directions of the γ-rays are given with reference to the crystal lattice. Fig.(10) shows the three amplitudes

S_n (n = 1, 2, 3) for the case of an axially symmetric EFG, whose V_{zz} component points either along a ⟨100⟩, ⟨110⟩ or ⟨111⟩ (horizontal row) lattice direction and the γγ coincidence (θ = 180°) is measured along one of the three major lattice direction. For comparison, also the S_n values for a randomly oriented EFG tensor (polycrystalline sample) are shown.

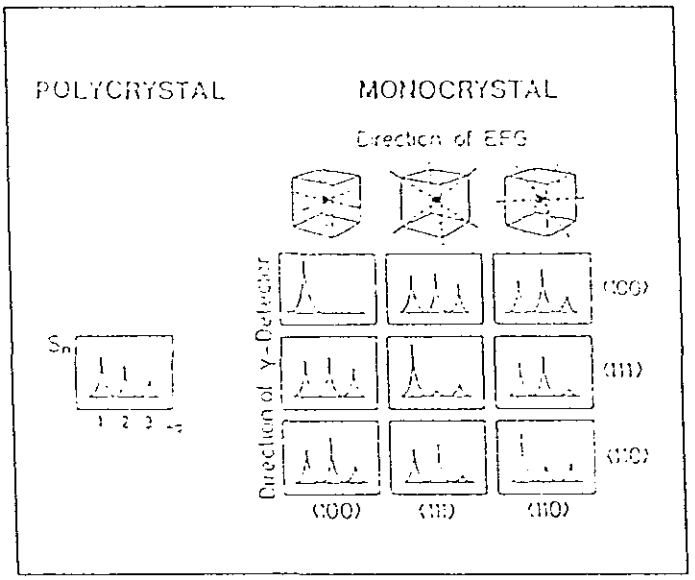

Fig. 10. *Influence of the orientation of the EFG on the spin precession amplitude* S_n *[29].*

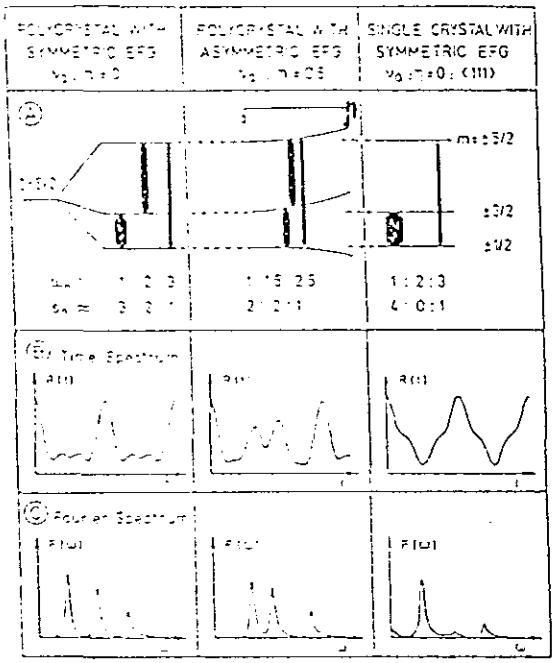

Fig. 11. *a) Level splitting for spin I = 5/2. b)PAC time spectra and c) their Fourier transform [29].*

Fig.(11) shows the electric quadrupole splitting for spin I = 5/2 caused by an electric field gradient with η = 0 and η = 0.5 in a polycrystalline sample. In case of a single crystal, an orientation of the electric field gradient and of the γ-detectors along ⟨111⟩ lattice directions are assumed correspondingly the amplitudes S_2 and S_3 are strongly reduced compared to the other two cases. In addition, are shown: (B) the time spectra exhibiting the corresponding perturbation factors $G_{kk}(t)$ and (C) frequency spectra.

2.3.2. Probe Atoms.

The prominent feature of a PAC experiment is the ability to observe the $\gamma\gamma$ angular correlation. For its application generally it requires a radioactive isotope that emits as a cascade two γ-rays that should be easily distinguishable by their different energies $E_{\gamma 1}$ and $E_{\gamma 2}$. In addition the radioactive isotope must satisfy the following requirements to be a probe atom for PAC experiment.

- The lifetime τ of the intermediate nuclear state determines the time window through which the spin precession can be observed. The upper and lower limits of the lifetime are imposed by the conditions that only one nucleus decays within the time window and by the limited time resolution of the experimental equipment respectively. Thus τ should lie between a few nanoseconds and microseconds (usually between 2ns and 1μs).

- The nuclear moment of the intermediate state should be large because its magnitude along with the strength of the electromagnetic field determines the actual spin precession frequency ω whose period $2\pi/\omega$ should not be larger than the lifetime τ.

- The angular correlation coefficients of the $\gamma\gamma$ cascade should be large because they determine the statistical accuracy of the deduced hyperfine parameters and the minimum detectable fraction of nuclei associated with them.

- The half-life time of the parent isotope or a metastable excited state should be long enough to dope the sample under study with the probe atoms and to perform special treatments like annealing after ion implantation or doping with other impurity atoms and, finally, for performing the PAC experiment itself.

- The parent isotope has to interact with defects to form a molecule-like complex. In compound semiconductors this normally requires a charged defect state in the gap.

The above mentioned requirements strongly restrict the number of candidates suitable as probe atoms for PAC experiment. The radioactive ^{111}In is the most commonly used PAC probe atom and its decay scheme is shown in fig.(12).

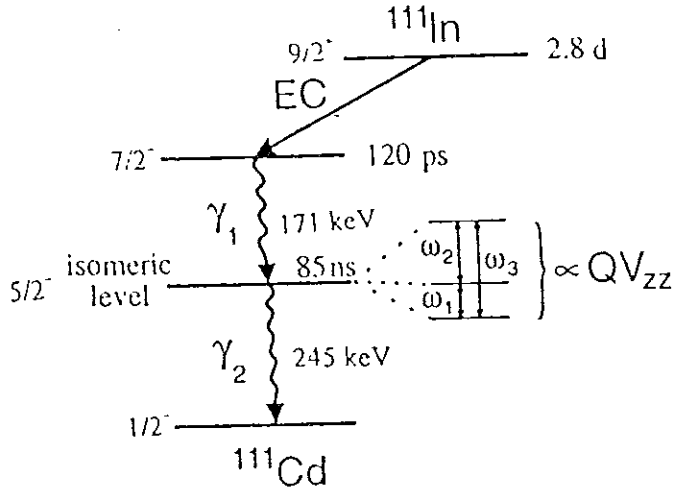

Fig. 12. *Nuclear decay scheme of the PAC probe atom ^{111}In decaying to ^{111}Cd via electron capture (EC). The hyperfine splitting of the isomeric level of ^{111}Cd populated by the first γ transition is used in the measurement of the electric field gradient [31, 32].*

The radioactive isotope ^{111}In with a half-life time of 2.8d via electron capture decay (EC) creates the excited ^{111}Cd daughter nucleus which comes to the ground state with the emission of two γ-rays, γ_1 and γ_2 having energies of 171 keV and 245 keV respectively. The isomeric intermediate nuclear state with I = 5/2 of ^{111}Cd is characterized by a quadrupole moment Q = 0.8 barn and a half-life time of 85 ns.

The parent isotope ^{111}In is commercially available in the form of carrier-free $^{111}InCl_3$ - solution and its half-life of 2.8d allows for about two weeks of experiment time on one sample. Both photons, γ_1 and γ_2, are separately detected by NaI crystals. The large angular correlation coefficient A_{22} along with suitable values of lifetime, magnetic dipole and electric quadrupole moments of the intermediate state guarantee an accurate determination of the hyperfine interaction parameters.

Thus the radioactive isotope ^{111}In fulfils the above described conditions almost perfectly and is found to be the most convenient probe atom for PAC experiment. For the II-VI compound semiconductors its chemical nature makes it to act as a donor and interacts with acceptor defects by forming a molecule like complex.

2.3.3. The PAC Spectrum

In principle two detectors tuned to record the first and the second photon of the $\gamma\gamma$ cascade respectively are enough to measure the angular correlation between γ_1 and γ_2 as a function of time elapsed between the arrival of both γ-rays. In order to measure the time difference between the detection of the two photons, one uses $t_{\gamma 1}$ and $t_{\gamma 2}$ to start and stop a clock which produces an analog pulse whose amplitude is proportional to the elapsed time Δt.

However 50% of the coincidence are wasted since a particular detector acts either as a start or a stop detector only. This can be improved to obtain higher detection efficiencies if each detector is to be used both for start and stop events. Usually, two more detectors are added thereby forming an array of four detectors, each of them enclosing an angle of 90° with its neighbour and form a cross with the sample (probe) at its centre.

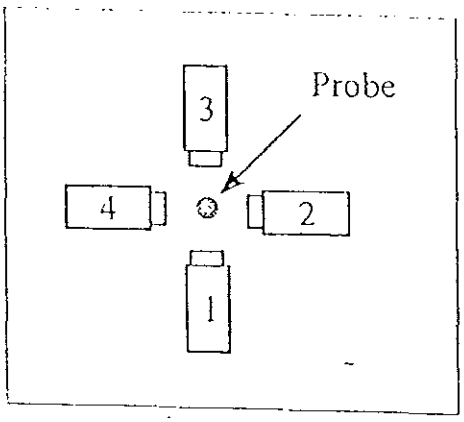

Fig. 13. *4 - Detector arrangement for a PAC apparatus [29].*

These four detectors allow us to record 12 coincidence spectra, four 180° and eight 90°, simultaneously. Designating by I_{ij} (θ,t) the coincidence spectrum recorded by detectors i and j (i, j = 1, ..., 4) forming the angle θ, after subtracting the time independent background of accidental coincidences, the following ratio can be formed out of four spectra [28].

$$\frac{I_{13}(180,t)I_{24}(180,t)}{I_{14}(90,t)I_{23}(90,t)} = \left(\frac{W(180,t)}{W(90,t)}\right)^2 \tag{2.23}$$

This combination eliminates the different efficiencies of the γ-detectors so that the factor I_0 in equation (2.18) along with the exponential decay $\exp(-t/\tau)$ cancels.

The angular correlation function for a random orientation of the local fields, see equation (2.19), and with Kmax = 2, is

$$W(\theta,t) = 1 + A_{22}G_{22}(t)p_2(\cos\theta) \tag{2.24}$$

with the Legendre polynomial $P_2(\cos\theta) = 1/3\ (3\cos^2\theta - 1)$, the perturbation factor $G_{22}(t)$ multiplied by the angular correlation coefficient A_{22} is easily obtained from the quotient of equation (2.23) [28].

$$R(t) = \frac{2}{3}\left(\frac{W(180,t)}{W(90,t)} - 1\right) \approx A_{22}G_{22}(t) \tag{2.25}$$

This ratio R(t) is usually called the PAC time spectrum. Its Fourier transform $F(\omega)$ shows the three frequencies ω_n connected with the electric field gradient tensor caused by a defect at the probe atom.

$$F(\omega) = \int_{-\infty}^{\infty} G_{22}(t)e^{i\omega t}dt \tag{2.26}$$

From the ratio ω_2/ω_1 the asymmetry parameter η (fig.9) and from ω_1 the component V_{zz} of the field gradient are obtained. In addition information on the orientation $\langle hkl \rangle$ of the EFG tensor, i.e., the coefficient S_n, can be obtained.

Recording a full PAC spectrum requires the detection of the angular correlation at many probe atoms. Probe atoms at different lattice sites in the same sample can experience different local fields i.e. they can be exposed to different microscopic environments. In this case the perturbation function reads [28].

$$G_{22}^{j}(t) = \sum_{j} f_j G^j(t) \tag{2.27}$$

where f_j is the relative fraction of probe atoms distinguished by its characteristic field gradient, i.e., by ν_{Qj}, η_j and a set of amplitudes S_{nj}. Then the time spectrum becomes

$$R(t) = A_{22} \sum_{j} f_j G_{22}^{j}(t) \tag{2.28}$$

If a certain fraction f of the probes is decorated with a uniform defect with $\eta = 0$ (axial symmetry), while the remaining fraction (1 - f) is located on sites with cubic symmetry, the PAC spectrum, R(t), takes the following form [28, 33].

$$R(t) = (1 - f)A_{22} + fA_{22}G_{22}(t) \tag{2.29}$$

i.e.,

$$R(t) = A_{22}\left((1 - f) + f \cdot \left(S_o + \sum_{n=1}^{3} S_{2n} \cos(\omega_n t)\right)\right) \tag{2.30}$$

This spectrum contains the information about the hyperfine interaction of the probe nucleus with the electromagnetic fields of its environment and it is obtained by measuring the coincidence rate of the two emitted γ-rays as a function of the time which passed between the detection of both γ-rays [34, 35].

Fig.(14) shows how the correlation in space and time between the two γ quanta arising from the same ^{111}In decay is detected using a standard four detector set up.

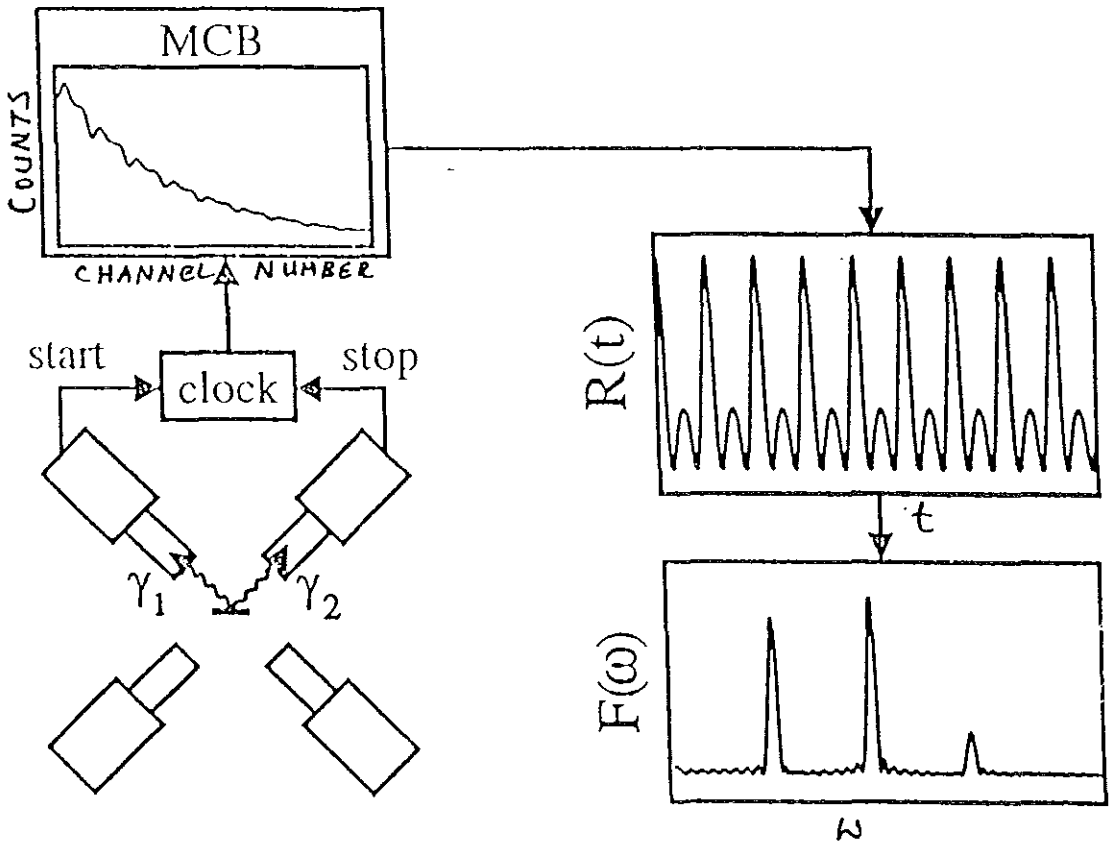

Fig. 14. *Schematic block diagram of a PAC measurement with four γ detectors [31].*

CHAPTER THREE

Experimental Apparatus

3.1. Function of the PAC Apparatus

As γ-detectors BaF_2 or NaI (Tl) crystals, coupled to a photomultiplier, are used. From each detector a "*slow*" and a "*fast*" signal are derived and subsequently used to measure the energy and to define the time at which the γ-quantum was detected.

From the dynode of the photomultiplier an energy proportional signal is given, which after passing through a pre-amplifier on the entrance is given to a main amplifier (Delay-Line-Amplifier, DLA). The DLA integrates the entrance signal and amplifies it on a variable amplifier factor. Through the application of Delay-Line-Shaping the signal will be formed, and a bipolar output signal will be fed into two Single Channel Analysers (SCA), set at the energy corresponding to the first and second gamma radiation.

The SCA filters out the 171 keV start line and the 245 keV stop line and delivers an exit signal with a defined energy and a width of about 200 ns. Since each detector is used both for start and stop event, two SCA, set at the corresponding energies $E(\gamma_1)$ and $E(\gamma_2)$ are required.

The anode signal of the photomultiplier is driven towards a Constant Fraction Discriminator (CFD). The CFD produces a standard time signal output pulse preceding the SCA pulse by typically 1-2 μs because of the integration time of the slow signal. So the processing time of the energy signal to get over, this time signal is delayed over a cable delay of 1.5 μs. Delaying the fast signal by this time, the SCA output pulses can be used - employing a fast overlap coincidence - to decide whether a discriminator output signal corresponds to a γ_1 or γ_2 quantum. This procedure is often called a slow (E_γ)-fast (t_γ) coincidence (SFC).

The time signal that comes out from the delay is given to an Octal Discriminator (OD) for further shaping to preserve the pulse amplitude information (analog signal) which was affected by the delay, as well as for coincidence level. Through additional delay of the energy signal in timely coincidence is brought. The coincidence level runs with an entrance signal, that the time information of the start and the stop results respectively.

The start and stop results of the coincidence level would be mixed with one another through a dual mixer (DM). The dual mixer is a logical unit that results an OR output. This blended start signal triggers on the start-entrance of Time-to-Pulse height Converter (TPC) and the blended stop signal after being delayed in a common delay line by a time of usually 30 ns, to see the time zero in spectra, triggers off the TPC corresponding to the stop entrance.

TPC, measures the time interval between pulses to its start and stop inputs and generates an analog output pulse proportional to the measured time. A VALID-START and a VALID-STOP output signals are provided for each accepted start and stop input, respectively. The VALID-START signal is transferred to a Gate-and-delay generator where a 4 μs broad and 5V amplitude gate-signal as TRUE-START signal is derived and is given to the Routing-Unit. The VALID-STOP over to another Gate-generator as TRUE-STOP signal is transferred to the Routing-Unit.

The start and stop signal of the coincidence level is also given to a level adapter after an adjustable delay of about 60 ns. The level adapter transforms the standared-NIM-signal of the coincidence-level into 5 V TTL-signal, which the chips of the Routing box can accept. The extra delay of the stop and start signal makes it possible for a time-coincidence with the TPC TRUE-START and TRUE-STOP signal. The Routing-Unit is set on by the TRUE-START and TRUE-STOP signal and then decides the detector combination which the TPC has started and stopped. This detector combination is fixed to a 4 bit-digit. After deciding on a detector combination, the

Routing-Unit announces to the Analog-Digital-Converter through ADC-Gate that it has a combination.

Now the ADC determines the channel number after digitizing the voltage signal of the TPC, and transfers this number to the Multi-Channel-Buffer (MCB). The MCB through a BUSY signal asks the Routing-Unit for the corresponding detector combination. The 4-bit digital signal of the Routing-Unit decides now the segment, in which the coincidence, start and stop, is counted. The segmentation of the MCB, in 16 equal segments, makes the reception of all the 12 coincident spectra possible.

Schematic representation of the foregoing discussion is illustrated in the next page.

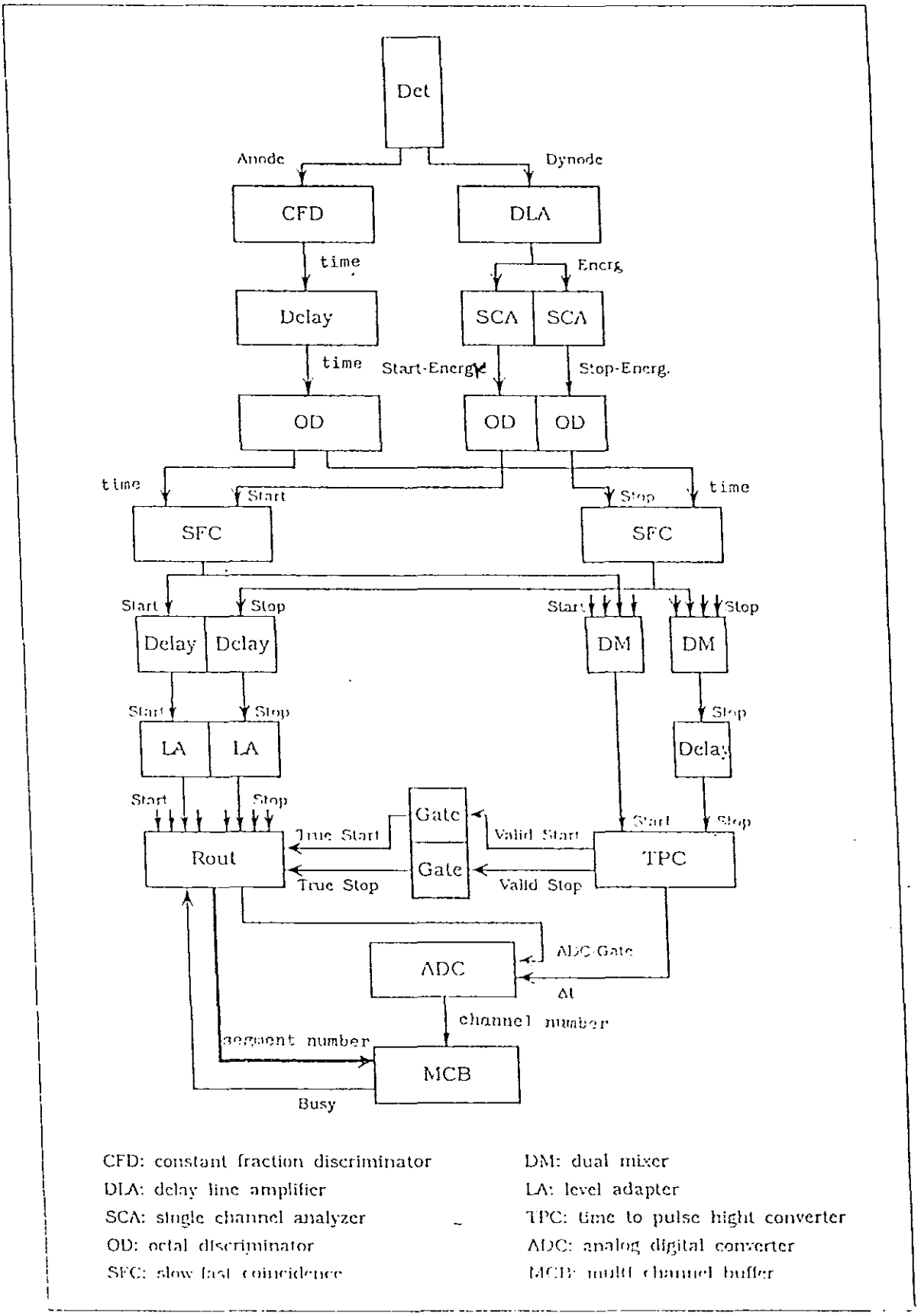

CFD: constant fraction discriminator
DLA: delay line amplifier
SCA: single channel analyzer
OD: octal discriminator
SFC: slow fast coincidence
DM: dual mixer
LA: level adapter
TPC: time to pulse hight converter
ADC: analog digital converter
MCB: multi channel buffer

Fig. 15. *Circuit Diagram for signal processing of a PAC apparatus [29].*

3.2. Components of a PAC - Equipment

DETECTOR

The scintillation detector consists of a scintillator crystal of BaF_2 or Thallium-activated NaI in conjunction with a photomultiplier tube. The scintillator crystals give off light in the visible and ultra-violet region when ionizing radiation passes into them and when viewed with a photomultiplier they are a very efficient detector of gamma-rays. The amount of light and consequently the output pulse height is proportional to the energy lost by the gamma-ray in the crystal. The scintillator crystal must be transparent to its own light.

The photomultiplier tube works on the same principle as the photoelectric cell in that photoelectrons liberated from the photocathode are accelerated to an electrode at a higher potential. Bombardment of metals by electrons causes emission of secondary electrons with multiplication of the electron current. By employing several such electrodes in cascade the photocurrent can be magnified by 10^6 or more. The photomultiplier tube has ten or more such electrodes which are called dynodes, each one being at a successively higher voltage than the previous one. The overall voltage between the cathode and the anode can be as high as 2 kV.

After conversion of the energy of the photon into a light flash by scintillator crystals which afterwards produces an electron avalanche in the photomultiplier, the resulting electronic signal is splitted and amplified, so that a "***slow***" and a "***fast***" signal are derived and subsequently used to measure the energy and to define the time at which the γ-quantum was detected. The scintillation detector can therefore be used to obtain the spectrum of a gamma-ray source.

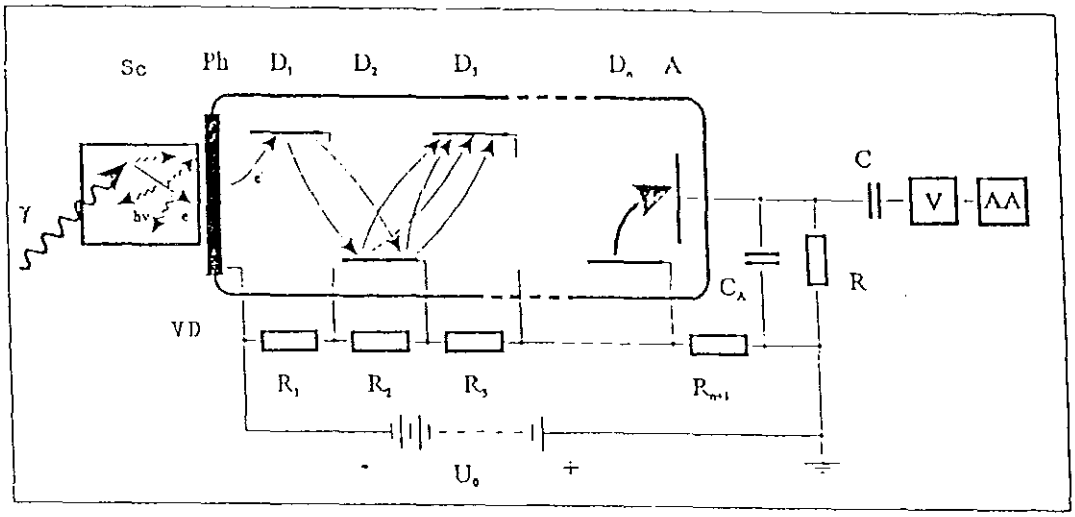

Fig. 16. *The working method and principles of Scintillation detector: Sc scintillator, Ph photocathode, D1 ... Dn Dynode, A Anode, VD voltage divider, CA anode capacitor [29].*

DELAY LINE AMPLIFIER (DLA)

Its primary purpose is to magnify the amplitude of the preamplifier output pulse. In addition, it shapes the pulses to optimize the energy resolution, and to minimize the risk of overlap between successive pulses.

The output of the preamplifier for each pulse consists of a rapidly rising step, followed by a slow exponential decay. It is the amplitude of the step that represents the energy of the detected radiation. Decay time constants of 50 μs are prevalent, but longer time constants are encountered on some preamplifiers.

In normal operation at ordinary counting rates, the step rise caused by each detector event rides on the exponential decay of a previous event, and the preamplifier output does not get the chance to return to the base line. Since the amplitude of detector events is usually variable and the time of occurrence is random, the preamplifier output is usually irregular as shown in the figure below.

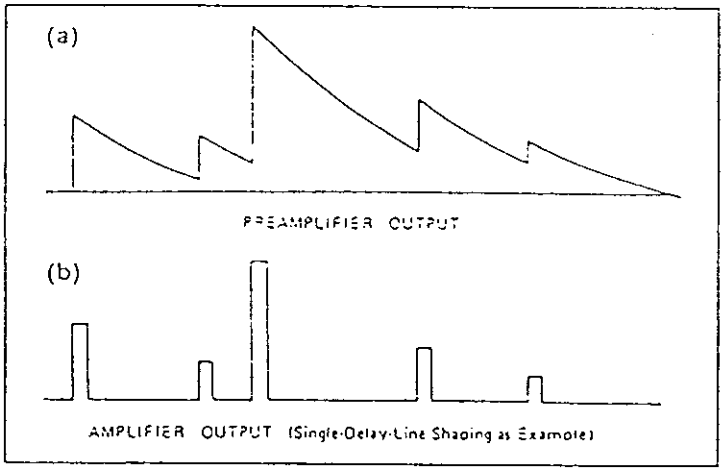

Fig. 17. *Output Pulse Shapes from (a) a Resistive - Feedback preamplifier, and (b) the Delay - Line shaping Amplifier connected to the preamplifier [36].*

Before amplification, the pulse-shaping amplifier must replace the long decay time of the amplifier output pulse with a much shorter decay time. Otherwise, the acceptable counting rates would be severely restricted. Amplifiers employing delay-line pulse shaping are well suited to the pulse processing requirements of scintillation detectors. The step pulse from the preamplifier is inverted, delayed, and added back to the original step pulse. The result is a rectangular output pulse with a width equal to the delay time of the delay line. In fact, the falling edge of the pulse is a delayed, mirror image of the rising edge. The energy information represented by the amplitudes of the steps from the preamplifier output has been preserved, and the pulses return to baseline before the next pulse arrives.

SINGLE-CHANNEL ANALYZER (SCA)

The selection of a range of signal levels at the output of a spectroscopy amplifier is equivalent to the selection of a range of energies of the nuclear events being processed. This selection can be accomplished in a nuclear measurement system by the use of discriminators and Single-Channel Analyzers (SCAs). A discriminator produces an output logic pulse only if its input signal exceeds a present threshold level. A Single-Channel Analyzer produces an output logic pulse only if the peak amplitude of its

input signal falls within the energy window that is established with two pre-set threshold levels.

Three primary modes of discriminator operation are available in SCAs - Integral, Normal and Windows.

Integral-mode

In the integral mode of operation, the SCA can function as integral discriminator in which the output signals are generated when the leading edge of the input signal crosses the discriminator threshold level. The SCA OUT is generated for all pulse amplitudes exceeding the lower level threshold.

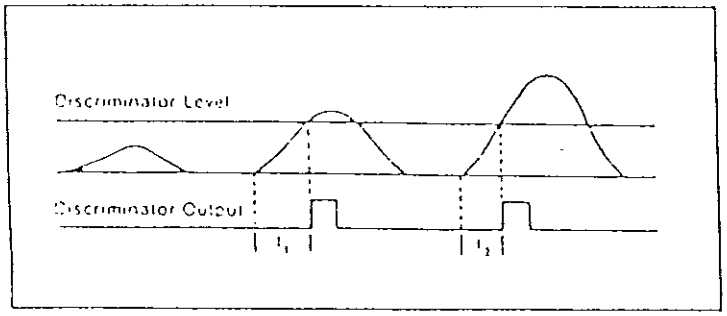

Fig. 18. *Formation of the output signal in Integral - Mode [36].*

Normal-mode

In the SCA normal mode of operation upper-level and lower-level thresholds exist and are independently adjustable. Removal of the upper-level discriminator restrictions from the SCA allows it to be used as an integral discriminator. The SCA OUT is generated for pulse amplitudes which exceeds the lower level threshold, but do not exceed the upper level threshold. For instance to filter out the 171 KeV start line and the 245 KeV stop line of the probe atom ^{111}In.

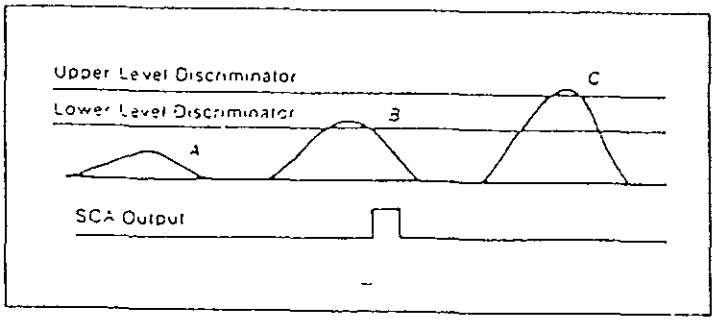

Fig. 19. *Function of SCA in Normal - Mode [36].*

Window-mode

In the SCA window mode, the upper-level threshold control is used to establish a voltage level that is added to the lower-level threshold voltage to yield the upper-level discriminator threshold level. Thus, when the lower-level setting is changed, the upper-level threshold changes by the same amount. An external voltage reference for the lower-level discriminator can be supplied to advance the window through a preselected range of pulse heights.

CONSTANT FRACTION DISCRIMINATOR (CFD)

The decisive thing for PAC measurement is the exact designation of the moment of an event where the difference between two events must be determined as exact as possible. The problem that we have is the formation of a logical signal that stands in a firm relation with the time point of the occurrence of an event. Thus, the time information represented by the amplitudes of these signals should be preserved through out the process. For the time point determination we have a CFD. It has the work of shaping the anode signal of the detector to a time sharp pulse signal by minimizing the effect of variations in the input signal amplitude.

The entrance of the constant fraction discriminator accepts signals from -5 mV to -5 V. But, to suppress noise a threshold exists so just signals with amplitude ranging from -5 mV to -1 V are accepted.

The pulse shaping used in a constant - fraction discriminator is shown below.

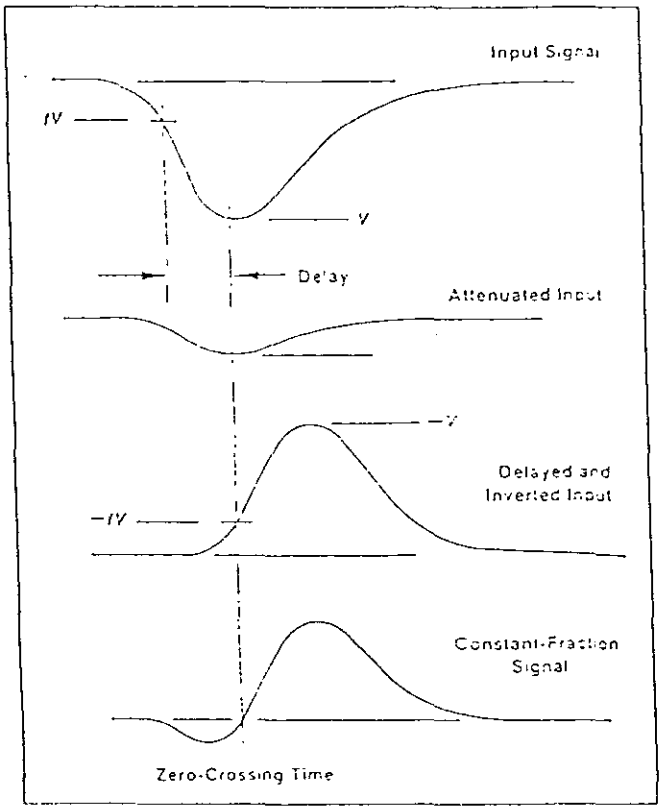

Fig. 20. *Formation of the Constant - Fraction signal [36].*

The input signal is split into two parts. One part is attenuated to a fraction f of the original amplitude, and the other part is delayed and inverted. These two signals are then combined to form the constant-fraction timing signal. Note: the delay is selected so that the optimum fraction of the delayed signal occurs at the peak amplitude of the attenuated signal. This causes the zero-crossing time of the constant-fraction bipolar signal to occur at the optimum fraction.

TIME TO PULSE HEIGHT CONVERTER (TPC)

TPC can be used to measure the time relationship between correlated or coincident events. A TPC converts the time interval between two timing logic signals into an output pulse with an amplitude that is proportional to the time interval.

Time-to-pulse height converters provide an output pulse with an amplitude proportional to the time interval between a start input and a subsequent stop input. The output is normally fed to an ADC to generate the time spectrum.

Timing experiments requiring time ranges of 10 ns to 2 ms may be performed with single-channel analysis, giving the experimenter unparalleled flexibility in analyzing random nuclear events that occur within a selected time range. Separate getting of the start and stop inputs eliminate unwanted events from the time spectra through externally imposed energy restrictions by the SCA.

Valid start and valid conversion outputs are provided for each accepted start and stop input respectively. The duration of the valid start output indicates the interval from the accepted start until the end of reset. Valid conversion occurs from the end of the internal delay after stop to the end of reset. The time-to-pulse height conversion signal is generated only after a start signal has initiated the conversion process and a stop signal has been received within the selected time range.

No output signals are generated by any start or stop signals out side the selected time range. Therefore, any start signal that is not accompanied by a stop signal within the selected range will produce no output signal.

ANALOG-TO-DIGITAL CONVERTER (ADC)

An analog-to-digital converter measures the maximum amplitude of an analog pulse and converts that value to a digital number. The digital output is a proportional

representation of the analog amplitude at the ADC input. For sequentially arriving pulses, the digital outputs from the ADC are fed to a dedicated memory, or a computer, and sorted into a histogram. This histogram represents the spectrum of input pulse heights. If the input pulses come from an energy spectroscopy amplifier, the histogram corresponds to the energy spectrum observed by the associated detector.

When the output of a time-to-pulse height converter is connected to the ADC input, the histogram represents the time spectrum measured by the time-to-pulse height converter. If a computer is employed to display the spectrum, then the combination of the ADC and the histogramming memory is called a Multi-Channel-Buffer (MCB).

ROUTING-UNIT

The Routing-Unit is a logical unit, which determines the start-stop-detector combination that had started or stopped the TPC. For each detector - combination a 4-bit number is assigned and is delivered to the MCB.

The start-respectively stop- incoming signals create a 100 ns broad TTL signal by means of impulse generation, and in turn this signal charges a start respectively stop flip-flop. In addition the start and stop signals mix together and can be used as test start and test stop. These test points helps us to check for the time coincidence of the incoming signals with the Gate-signals.

Once the TPC is started, its valid start signal produces a gate signal as TRUE-START through a Gate-Generator. The rising side of this gate signal times the start flip-flop, so that this stored signal gives a coincidence level. Analogously, a stop of the TPC produces a valid conversion-signal which is given to the Rouiting-Unit as TRUE-STOP gate. The rising side of the true-stop signal measures the corresponding stop flip-flop that the stored stop-signal is given to the coincidence level. The falling side of the true-stop signal then resets both flip-flops.

The resulting coincidence level determines the start-stop-detector combination and transfers it to a decimal-binary converter that assigns a 4-bit number to the respective detector combination. An output flip-flop stores the determined detector combination until it is read by the MCB.

The coincidence signal through ADC-Gate activates the ADC, and now the ADC converts the voltage value of the TPC into a digital number and transfers it to the MCB. As soon as it receives this number the MCB asks through a "*BUSY*" signal to the Routing-Unit in which segment the event should be counted. This BUSY- signal times the output flip-flop of the Routing-Unit, and the stored 4-bit number is given to the MCB as segment-number.

Additionally, a switch enables the MCB for a pre-selection of the activated segments. In this case a binary-decimal-counter decodes the 4-bit number and compares it with the activated segments at the segment-control-Bus. If the segment - number is not allowed, then the output flip-flop of the Rouiting-Unit will be reset. This option then makes it possible to switch on/off segments during a measurement.

THE MULTI-CHANNEL-BUFFER (MCB)

For the reception of the time-spectra, a Multi-Channel-Buffer with an integrated ADC is used. The voltage-value of the TPC is digitized by the ADC, and this digital number serve to address the data channel in which the measured events should be counted.

In our PAC apparatus an ADCAM Multi-Channel-Buffer is being used, which enables us for a simultaneous consideration of twelve time spectra and on line output to a computer for evaluation.

This MCB has 8 . 2^{10} data memories and each of them contains a 24-Bit-word. The first bit is used to activate the channel and the rest 23 bits are available in order to store the value. The maximum counting rate of one channel is therefore limited to 2^{23}.

The data memory can be divided into 2, 4, 8 and 16 equal segments. To be able to take simultaneously all the twelve time spectra of the 4-detector combination, the partition into segments with each containing 512 channel is used.

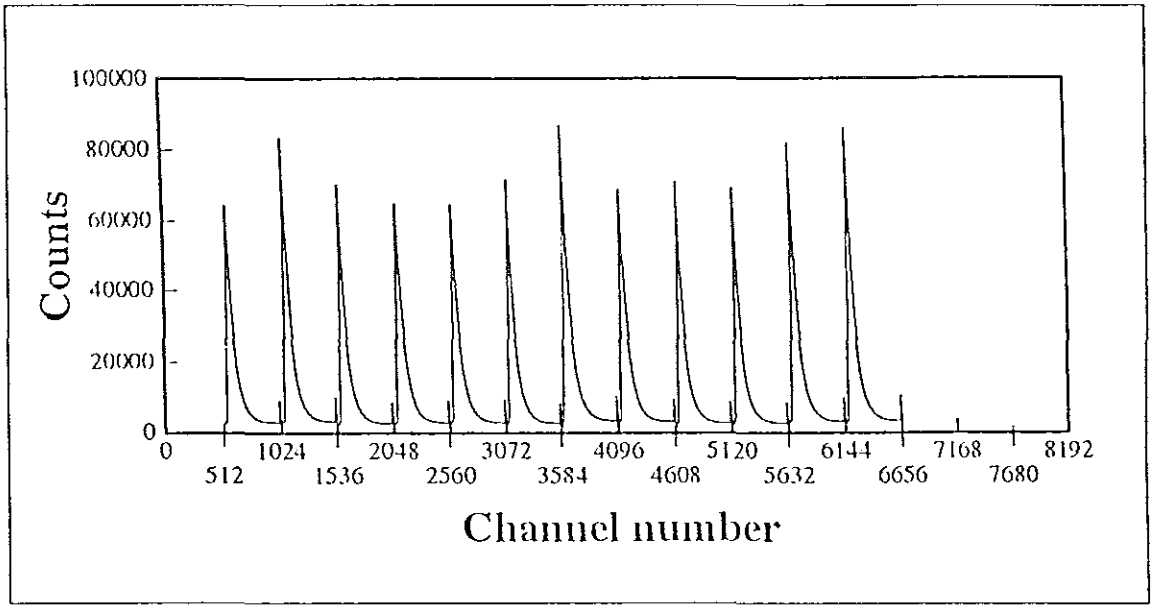

Fig. 21. *The content of the memory of the MCB after measurement [29].*

During a PAC measurement the MCB is being operated in the coincidence mode that is selected by a switch. In the coincidence mode the ADC does not function unless it is timed by a gate signal. This signal is delivered by the Routing-Unit when it has found out a detector combination. The ADC reads the voltage-value of the TPC after receiving the ADC-Gate signal, otherwise it does not work.

The ADC accepts voltage-values between 0 V and 10 V and converts them into a 13-Bit-number. The ADC is able to process at maximum counting rates of 100 KHz since the time of the conversion is about 10 μs.

A FIFO-Buffer (first-in-first-out) is composed of 40 slide registers and is working as an intermediate storage between the ADC and the MCB. The ADC output signal is therefore preserved until the MCB uses it for addressing the Routing-Unit. Through the FIFO the MCB can be read during a measurement without any interruption of its communication with a computer.

If the ADC has transferred the channel number to the MCB, then the MCB sends a BUSY signal to the Routing-Unit. The busy signal times the output of the output flip-flop of the Routing-Unit and the stored 4-bit number is passed to the MCB as segment number. The MCB just counts the event in the corresponding segment of the channel that is being determined by the ADC signal.

Segment number	1	2	3	4	5	6	7	8	9	10	11	12
Start-Stop comb.	1 - 3	1 - 4	2 - 3	2 - 4	3 - 1	3 - 2	4 - 1	4 - 2	1 - 2	2 - 1	3 - 4	4 - 3
Spectrum	180°	90°	90°	180°	180°	90°	90°	180°	90°	90°	90°	90°

Fig. 22. *The assignment of detector combination to the segment of the MCB [29].*

CHAPTER FOUR

Thermodynamical Investigation of the Metal Vacancy in ^{111}In Doped ZnSe

4.1. MOTIVATION.

The principal driving force towards a profound investigation of the II-VI materials in general and ZnSe in particular is the report of p-type ZnSe which might become a candidate for the blue-green laser diode [1]. As discussed in chapter one, section two, large scale application of ZnSe semiconductor technology has been restricted by doping problems. This requires a deep understanding of impurity atoms and lattice defects, either intentionally introduced into high purity material or involuntarily incorporated during some process steps. Due to Coulomb interaction electrically active centres can form close donor-acceptor complexes, resulting in an uncontrolled annihilation of the charge carriers. Understanding the nature and basic properties of these defects can help to achieve a more efficient defect control and even a utilisation of defects [37, 38].

In order to obtain a fundamental understanding of the doping mechanisms involved, atomistic information on these defects is necessary [1]. Thus, the PAC technique, which gives microscopic and local information due to the rapid decrease of the electric field gradient (EFG) with increasing distance from the probe atom, can be employed to exploit information on an atomic scale. In the sphere of our work the semiconductor ZnSe will be examined after diffusion of the radioactive donor ^{111}In which is the well known probe atom for PAC.

Because of the donor character of the ^{111}In probe atom and due to the positive binding energy that exists, intrinsic defects like the metal vacancy, the interestial chalcogen atom and p-type dopant atoms can be trapped and form close donor-acceptor pairs.

4.2. Sample Preparation:

4.2.1. Introduction.

A common procedure in introducing electrically or optically active defect centers into solids is to diffuse the appropriate foreign impurity or stoichiometric excess of a lattice constituent into the material until the whole volume of the specimen is uniformly doped. This is particularly true in the case of II-VI compounds, rearrangements occur inside the crystal during such a diffusion process. Native defects may diffuse in along with the foreign impurity or the diffusant may associate it self with such defects already present in the crystal.

To dope a ZnSe crystal with the respective probe atom, two different procedures are quite possible. These are:

1) Implantation of accelerated radioactive atom into the sample. The advantage of this is its applicability to all isotopes even in the case of low solubility. However, it requires an expensive facility, and a further problem is the radiation damage created during implantation.

2) Thermal treatment of the sample, so that the probe atoms are introduced, via diffusion or melting. This leads to a well-defined substitutional state of the impurity in the respective crystal. In our experimental work the second procedure has been employed and the steps of the preparation are as follows.

4.2.2. Experimental Procedure.

From a crystal bar of ZnSe, single crystalline ZnSe slices ($3 \times 3 \times 0.5 mm^3$) have been cut with ⟨111⟩ crystal orientation. The samples were etched by soaking in a saturated HCl solution for about 20 seconds to remove surface impurities and native oxides. They were then sealed in cleaned quartz capsules of 1 cm diameter and about 10 cm length with a solution of $^{111}InCl_3$: HCl in dried form and evacuated to about 10^{-5} bar.

To obtain a quantitative incorporation of ^{111}In into the crystal, the diffusion was performed under selenium over pressure. The samples were then annealed at 1068 K for 15 h to diffuse in the In and were cooled by fast immersion of the closed quartz capsule into water. The measured transition rates of the radioactive In into the crystal showed that more than 85% of the In was diffused into the ZnSe samples and the activity of the samples after diffusion was about 35 μCi. The overall diffusion process resulted in incorporating In to a considerable depth (more than 5 μm), which is deep enough to perform a PAC measurement. The In concentration in the samples was then about 10^{15} cm^{-3}. The samples were subsequently annealed for 30 min at a temperature of 787 K for the first isochronol annealing (no. 25a) and at about 709 K, based on the data of fig.(28), for the rest of the measurements as a post treatment and were quenched with a high cooling rate, i.e. dropping the very sample into water by breaking the quartz ampoule.

The post treatment was done, firstly to remove the selenium atoms which are supposed to be present on the surface of the crystal after diffusion and may have considerable influence on the subsequent measurements; secondly to have a low starting fraction i.e. in order to dissolve (as far as possible) those pairs which were formed during a slow cool after sample preparation, specially for isothermal annealing in order to observe the increasing of the pairing with annealing time.

Note that, since the diffusion process involves radioactive sources, in general, one should obey the following safety rules to reduce the exposure resulting from a given application [41].

a) Use low radioactive source.

b) Keep as far away from the radioactive source as possible, and only approach it when necessary to make adjustments.

c) Minimize time of exposure.

d) Shield well the radioactive source.

Subsequently the $\gamma\gamma$ perturbed angular correlation was recorded for about seven hours, on average, at room temperature for the 171-245 keV γ cascade in ^{111}Cd by means of a conventional four detector set-up as shown in fig.(14). Thus, the interaction of the 5/2 isomeric nuclear state of ^{111}Cd with an extra nuclear electric field gradient tensor can be observed. The measured 12 coincidence spectra are combined to one PAC spectrum, R(t), and equation (2.29) is fitted to this time spectrum using a least squares routine to determine the relative fraction f of In probe atoms associated with a specific defect characterised by a specific EFG, the quadrupole interaction frequency ν_Q associated with the EFG and the asymmetry parameter η of the EFG [42, 43, 44]. All the PAC measurements were performed at room temperature. Specific information on the diffusion condition of each sample, and the values for the measured fractions are tabulated in the Appendix.

The diffusion of ^{111}In into the ZnSe samples was done in the presence of Chlorine, which also acts as a donor by occupying the chalcogen site. In order to investigate the effect of chlorine on the experimental results, comparison was done with the experimental PAC data following doping with ^{111}In by ion implantation, a procedure that excludes an unintentional doping with chlorine. However, the experiments did not indicate any influence of chlorine on the results [1].

The orientation of the largest component of the EFG tensor (V_{zz}) for ZnSe is known, and it is along $\langle 111 \rangle$ lattice direction [1].

4.3. Results And Discussion.

The PAC spectroscopy measures the hyperfine interaction of the electric field gradient with radioactive ^{111}In nuclei that are incorporated into the sample. The EFG tensor can be specified completely; it is an integral quantity (*"fingerprint"*) of the charge distribution very close (<< 1 nm) to the probe atom [45]. In all experiments presented, the probe nucleus ^{111}Cd, originating from the electron capture (EC) decay of ^{111}In is used. Therefore the trapping and detrapping of the acceptors at the probe atom is governed by the properties of the indium atom. The EFG, however, is measured at the cadmium nucleus immediately after the decay, thus, yielding information about the electronic structure of the corresponding Cd-acceptor pairs.

The PAC measurements on the ZnSe samples after doping with ^{111}In (fig.(23)) ensure that the probe atoms are located in an unperturbed metallic lattice site (V_{zz} = 0, η= 0), as expected for substitutional atoms in a cubic environment. The spectrum does not show a modulation but rather a slight decrease of anisotropy with time.

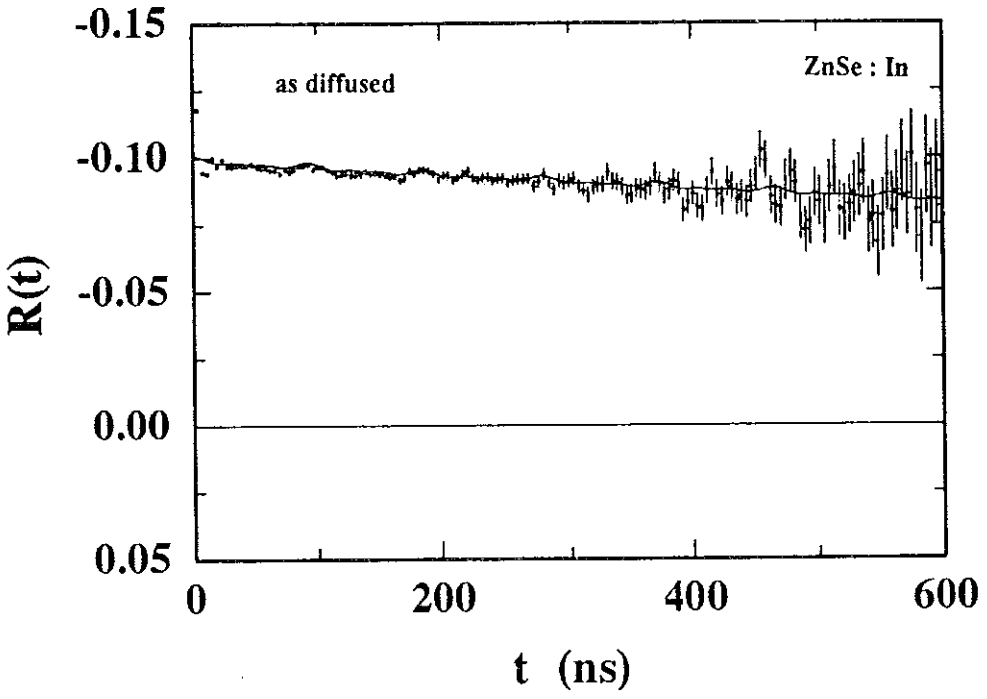

Fig. 23. *PAC Spectrum after diffusion of ^{111}In.*

However, after annealing above 300 K pronounced modulations with unique EFG are visible that indicate the presence of a defect at the probe atom. In fig.(24) the PAC time spectra R(t) (left-hand side) along with their Fourier transforms F(ω) (right-hand side) taken at different temperatures show that In-defect pairs are formed in ZnSe crystals.

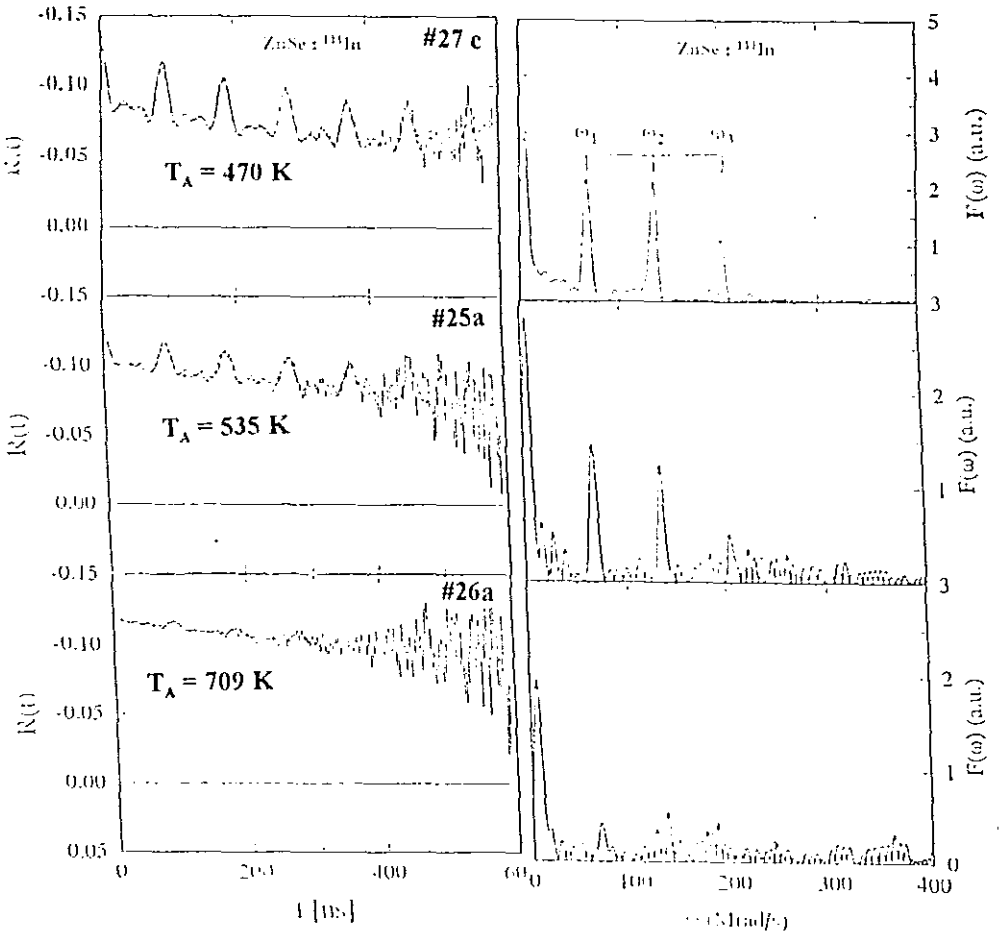

Fig. 24. PAC time spectrum and their Fourier transform recorded at room temperature after diffusion of ^{111}In and annealing at a temperature T_A.

Both R(t) spectra and their Fourier transform indicates the presence of a sharply defined frequency triplet which is found to recur within statistical error in all spectra investigated. The fact that the frequency ratio ω_2/ω_1 is slightly below 2, the value expected for axial symmetry ($\eta = 0$), indicates a slight deviation of the EFG tensor from

axial symmetry. The observed EFG is characterised by the coupling constant ν_Q = 72 MHz extracted from this experiment with the asymmetry parameter η = 0.05. The EFG described by this coupling constant is found to be specific for the presence of a metal vacancy V_{Zn} next to the ^{111}In probe atom that form $^{111}In_{Zn}$-V_{Zn} pairs [1]. Note also that the experimentally observed anisotropy coefficient A_{22} (as shown in the PAC spectra above) is A_{22} = -0.14 which is somewhat smaller than the theoretical value mainly due to the finite solid angle of the γ-ray detector.

The experiment was repeated for several samples of ZnSe undergone the same diffusion process. In all cases, only the presence of metallic vacancy has been observed, that is all spectra yielded the same ν_Q = (72 $\pm$1) MHz. Whereas, other possible acceptor defects, such as the chalcogen interestitial atom Se_i or the anti site defect Zn_{Se} have not been found; reasons might be either their neutral charge states or their too low concentration [1].

The formation of metallic vacancies was just to counterbalance the affected stoichiometry of the ZnSe crystal due to the increased fraction of Se atoms meant to enhance the diffusivity of ^{111}In into the crystal. Of course, the increased Se concentration might as well produce Se_i instead of V_{Zn} defects. In this case, however, it would be difficult to explain the enhanced incorporation of the radioactive ^{111}In atoms into the crystals. Similarly, the antisite defect ZnSe, is excluded because of the observed stoichiometric effects; that the concentration of the defect is increased in Seienium - rich crystals but decreased in Zn rich crystals [1].

The largest component V_{zz} of the observed field gradient due to In_{Zn}-V_{Zn} pairs was experimentally determined to point along a $\langle 111 \rangle$ lattice direction and the proposed model for the geometry of In_{Zn}-V_{Zn} pair is shown in fig.(25).

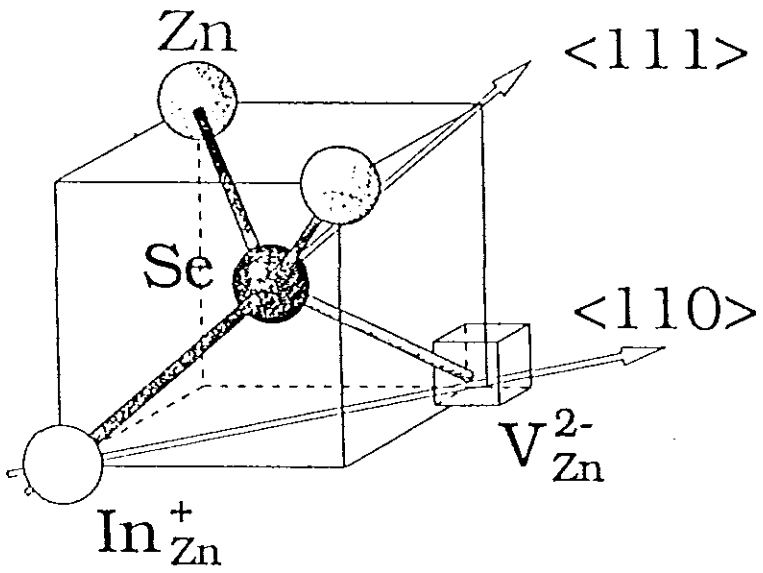

Fig. 25. *Proposed model for the geometry of the In_M-V_M pairs in ZnSe. The ⟨111⟩ orientation of the measured EFG tensor indicates a rearrangement of the electronic charge distribution about the Se atom [1].*

Since the EFG is sensitive to the deviation in the charge density from spherical symmetry, the ⟨111⟩ orientation of the tensor shows that the extra charge causing the vacancy associated EFG is located in the ⟨111⟩ direction, most probably close to the site of the Se atom being nearest neighbour to the ^{111}In probe atom [1].

4.3.1. Temperature Dependence Of In-V Pair Concentration.

The formation of pairs (or complexes) of impurities in semiconductors requires both an attractive interaction between them and a sufficiently high mobility of at least one of the atoms. For donor-acceptor pairing, the first condition is fulfilled by the Coulomb attraction of the charged impurities, and the second condition requires a particular temperature (550 K in ZnSe), in detail depending on the concentration and diffusivity of the atoms. Therefore the pairing process is investigated by annealing experiments.

The thermal stability of the In_{Zn}-V_{Zn} pairs is obtained by measuring their absolute fraction f, i.e., the amplitude of modulation of a PAC spectrum, during an isochronal

annealing sequence. The relative fraction of probe atoms associated with the defect is given by

$$f = \frac{[In_{Zn} - V_{Zn}]}{[In]} \tag{4.1}$$

Thus, (1-f) describe the fraction of In atoms without a defect. Based on the formation and dissociation of the pairs with temperature, the migration energy E_m of the metal vacancy and its binding energy E_b with the donor In can be determined.

The data points in fig.(26) represent the relative pair fractions measured after heating an ^{111}In doped ZnSe crystal to the respective temperature T_A for 30 min in vacuum and quenching into water at 300 K. Specially, the first data point was prepared by annealing at 786 K for 30 min in vacuum and quenching with a high cooling rate 10^3-10^4 Ks^{-1}.

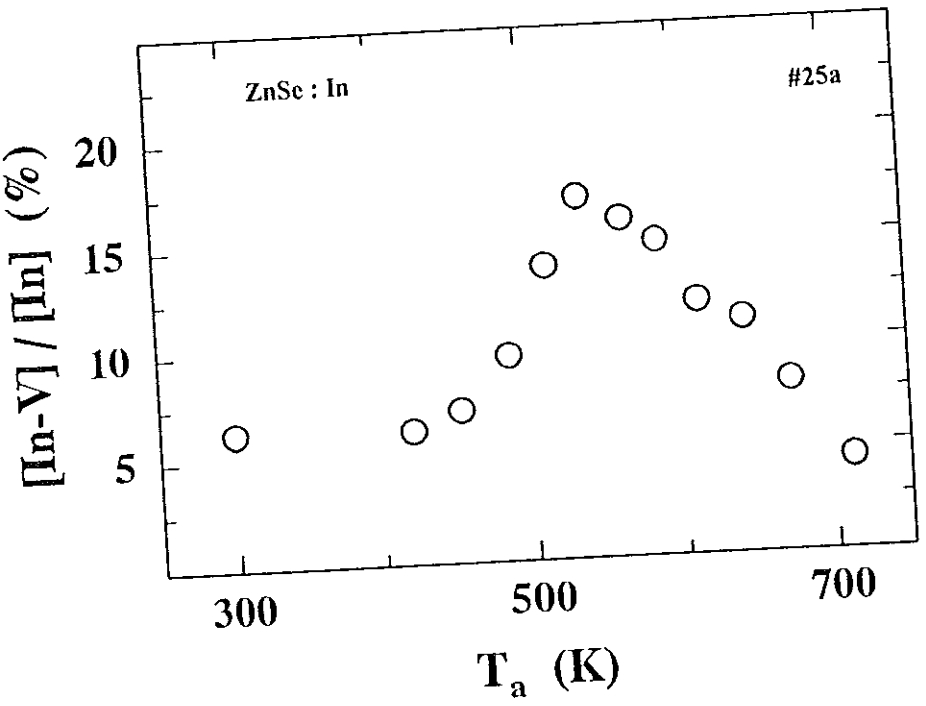

Fig. 26. Percentage of ^{111}In atoms in In_{Zn}-V_{Zn} complexes as a function of annealing temperature for the sample annealed in vacuum for 30 min [Isochronal annealing].

Annealing up to 535 K resulted in an increase of the pair fraction to f = 0.17. This is obviously, due to the existence of isolated vacancies that were frozen by the first

quench from 786 K and were now mobilised and trapped by the In atoms. The decrease in the pair fraction above 535 K is attributed to the finite binding energy between In_{Zn} and V_{Zn}, so that annealing at a higher temperature leads to the break up of the complexes. Furthermore, by comparing the data of fig.(26) with the experimental work of Wichert et al [1], the majority of the vacancies are found to be mobilised and trapped by the In atoms at temperatures around 550 K and thus we can have a feeling on the local vacancy concentration around ^{111}In atoms.

Thermodynamical Model Of In-V Pairing.

The PAC data show that the ZnSe crystals contain only isolated In atoms and In-V pairs, i.e., total indium concentration:

$$[In] = [In - V] + [In_{iso}] \tag{4.2}$$

Thus, the experimental data in fig.(26) can be described by the following reaction

$$In_{iso} + V_{iso} \overleftrightarrow{\rightarrow} (In - V) \tag{4.3}$$

Where, the forward reaction represents the formation of pairs due to the existence of isolated vacancies and isolated indium atoms, while the reverse reaction shows the dissociation of pairs to their constituents.

All the PAC data are understandable in a consistent way using the following first order rate equation [46].

$$\frac{d}{dt}[In - V] = \lambda_f[In_{iso}] \cdot [V_{iso}] - \lambda_d[In - V] \tag{4.4}$$

Where $[V_{iso}]$ is the concentration of isolated vacancies, λ_f and λ_d are formation and dissociation coefficients respectively and are defined as follows:

$$\lambda_f = \Omega_t \cdot \nu_o \cdot \exp\left(\frac{-E_m}{kT}\right) \tag{4.5}$$

$$\lambda_d = \nu_o \cdot \exp\left(-\frac{E_b + E_m}{kT}\right) \tag{4.6}$$

where, E_m : migration energy of V_{Zn}

E_b : binding energy of V_{Zn} with the donor In.

ν_o : attempt frequency.

Ω_t : trapping volume.

From equation (4.4) we see that the rate of formation of pairs can be explicitly explained by the existence of isolated In atoms and isolated vacancies which either form pairing or are the result of dissociation. The formation of pairs (λ_f) is governed by the migration energy of V_{Zn} and the trapping volume Ω_t, which represents a region around an In atom in which a metallic vacancy will most likely be trapped if it is in this region; whereas the dissociation of pairs (λ_d) depends on binding energy plus migration energy.

By explicitly solving the rate equation, the relative fraction of In atoms involved in the pairing can be expressed as a function of the parameters which are involved in equation (4.5) and (4.6). Using equation (4.2) the rate equation can be written as

$$\frac{d}{dt}[In - V] = \lambda_f[In - V]^2 - \lambda_f[In - V]([In] + [V]) - \lambda_d[In - V] + \lambda_f[In][V] \tag{4.7}$$

where,

$$[V] = [V_{iso}] + [In - V] \tag{4.8}$$

On dividing both sides of equation (4.7) by the total In concentration and with the help of equation (4.1), this can be written as

$$\frac{df}{dt} = \lambda_f[In](1-f)\left(\frac{[V]}{[In]} - f\right) - \lambda_d f \tag{4.9}$$

Or,

$$\frac{df}{dt} = \lambda f^2 - \lambda\alpha f + \lambda\beta \tag{4.10}$$

where :

$$\lambda = \lambda_f[In]$$

$$\alpha = \frac{\lambda_d}{\lambda_f[In]} + \left(1 + \frac{[V]}{[In]}\right) = \frac{\lambda_d}{\lambda} + (1 + \beta) \tag{4.11}$$

$$\beta = \frac{[V]}{[In]}$$

In this case the decay of In within the annealing time of 30 min was not taken into account. At thermal equilibrium, df/dt = 0, and the corresponding expression for the fraction is

$$f_e = \frac{1}{2}\left\{\alpha - \sqrt{\alpha^2 - 4\beta}\right\} \tag{4.12}$$

Then equation (4.9) can be written as

$$\frac{df}{dt} = \lambda(f - f_e)\left(f - \frac{\beta}{f_e}\right) \tag{4.13}$$

hence,

$$\int \frac{df}{(f-f_e)\left(f-\frac{\beta}{f_e}\right)} = \lambda t + const. \tag{4.14}$$

On carrying out the integration we obtain

$$f = \frac{\left(f_e + \frac{\alpha}{f_e}\cdot C\cdot\exp(\frac{-t}{\tau})\right)}{(1+C\cdot\exp(\frac{-t}{\tau}))} \tag{4.15}$$

where C is an arbitrary constant, and τ is called the time constant and has the following form

$$\frac{1}{\tau} = \lambda\sqrt{\alpha^2 - 4\beta} \tag{4.16}$$

In order to obtain the constant C it is sufficient to consider equation (4.15) at t = 0. In this case we have

$$f = \frac{f_e + C\cdot\frac{\alpha}{f_e}}{1+C} = f_o \tag{4.17}$$

Where f_0 is called the starting fraction. Then the constant C can be shown to be

$$C = \frac{f_e - f_o}{\frac{\beta}{f_e} - f_o} \tag{4.18}$$

On substituting this expression into equation (4.15) and making some rearrangements, we obtain the required fraction f as a function of t and τ as follows:

$$f(t,\tau) = f_o + \frac{(f_e - f_o)\cdot\left(\frac{\alpha}{f_e} - f_o\right)\cdot(1 - \exp(\frac{-t}{\tau}))}{\left(\frac{\alpha}{f_e} - f_o\right) - (f_e - f_o)\exp(\frac{-t}{\tau})} \tag{4.19}$$

We see that for longer duration (compared to τ) of annealing time t the fraction f will have the thermal equilibrium value f_e. When we fit equation (4.19) to the experimental data, the required thermodynamic parameters E_m and E_b of the metallic vacancy V_{Zn} can be obtained.

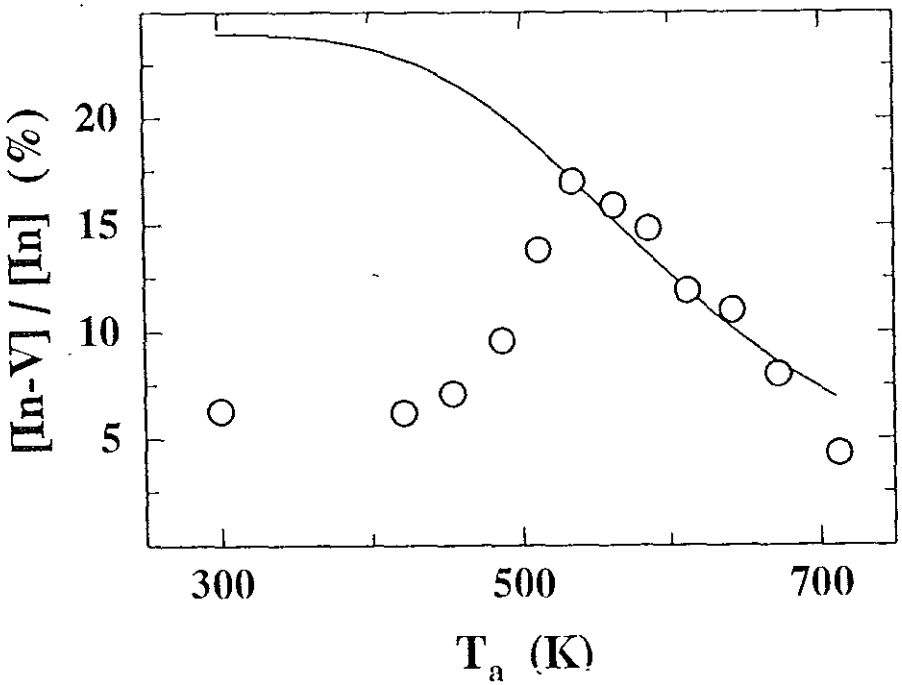

Fig. 27. *The solid line represents the fit of equation (4.19) to the data of fig. (27) for thermal equilibrium.*

The solid line in fig.(27) represents the fit of the solution of equation (4.19) for thermal equilibrium to the data of fig.(26). In the fitting process the attempt frequency ν_o is taken to be the typical phonon frequency of 10^{13} s^{-1} and the values used for the migration energy and binding energy of the metal vacancy was based on the experimental work of Wichert et al [1]; and these values are considered for comparison purposes at the end of this section.

As we see, for temperatures above 535 K (dissociation region) the 30 min annealing time is long enough to reach thermal equilibrium, whereas for temperatures below it (formation region) we observe big deviations from the thermal equilibrium value. That means for temperatures below 535 K the 30 min annealing time does not suffice to attain thermal equilibrium; and increasing the annealing time would result a corresponding increase in the pair fraction till we reach thermal equilibrium. Indeed, this gave birth to the idea of performing isothermal annealing with which we can observe the formation of pairs and hence gather information about the migration energy.

In the process of isothermal annealing we expect an increase in the defect complex with annealing time, and this is found to be strongly dependent on starting fraction, the temperature, and the thermal equilibrium value f_e for the selected temperature. In short, the difference between the starting fraction f_0 and the equilibrium value f_e should be large enough to observe the increment in the pair fraction with annealing time. This means in effect that there should be a large number of isolated vacancies around the In atoms that has to be mobilised and trapped by the In atoms during the process. Ultimately the temperatures chosen for isothermal annealing and of course for post treatment play the great role.

The selection of temperature for isothermal annealing was made based on the time constant, in which the time constant for the selected temperature should be long enough to perform a reasonable number of data points before the sample reaches at thermal equilibrium. Obviously, the selected temperature in general should be less than 535 K, at which thermal equilibrium is achieved within few seconds. However, to select a temperature for post treatment we have to study the behaviour of vacancy concentration (local) with temperature.

Fig.(28) shows the relative pair fractions measured after heating the ZnSe crystal at the respective temperature T_A for 30 min in vacuum and fast quenched, then annealed for 30 min at about 554 K to provide a large fraction of In probe atoms in the defect complex. At this juncture, bear in mind that the data of fig.(28) and fig.(26) were obtained on the same ZnSe sample (no. 25a), where the data of the former were performed following the isochronal annealing measurement. Note also that this experiment has been carried out within a very short time.

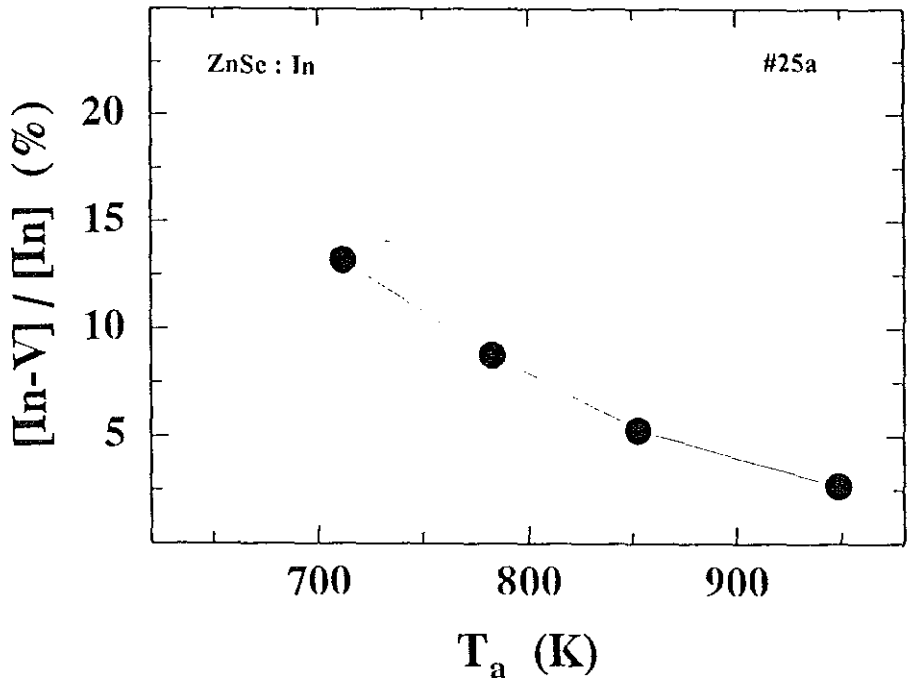

Fig. 28. *Relative fraction of* In_{Zn}-V_{Zn} *pairs obtained after annealing of ZnSe sample at the respective temperature* T_A *for 30 min, then annealed at about 554 K for 30 min.*

As we see in the figure local vacancy concentration decreases with increasing temperature. I contest that the cause for the observed decrease of vacancies which form pairing with the In atoms at higher temperatures under the specified conditions is attributed to either vacancies leave out of the crystal due to their high mobility in comparison with the In atoms or they might be in the bulky crystal but far away from In atoms. Since In atoms concentrate near the surface, 5μm deep, of the sample they give us no information about deeper vacancies. Since our interest is to have as large a number of vacancies as possible that have to be mobilised and form pairing with the In atoms; the temperature 709 K was selected for post treatment than the 787 K.

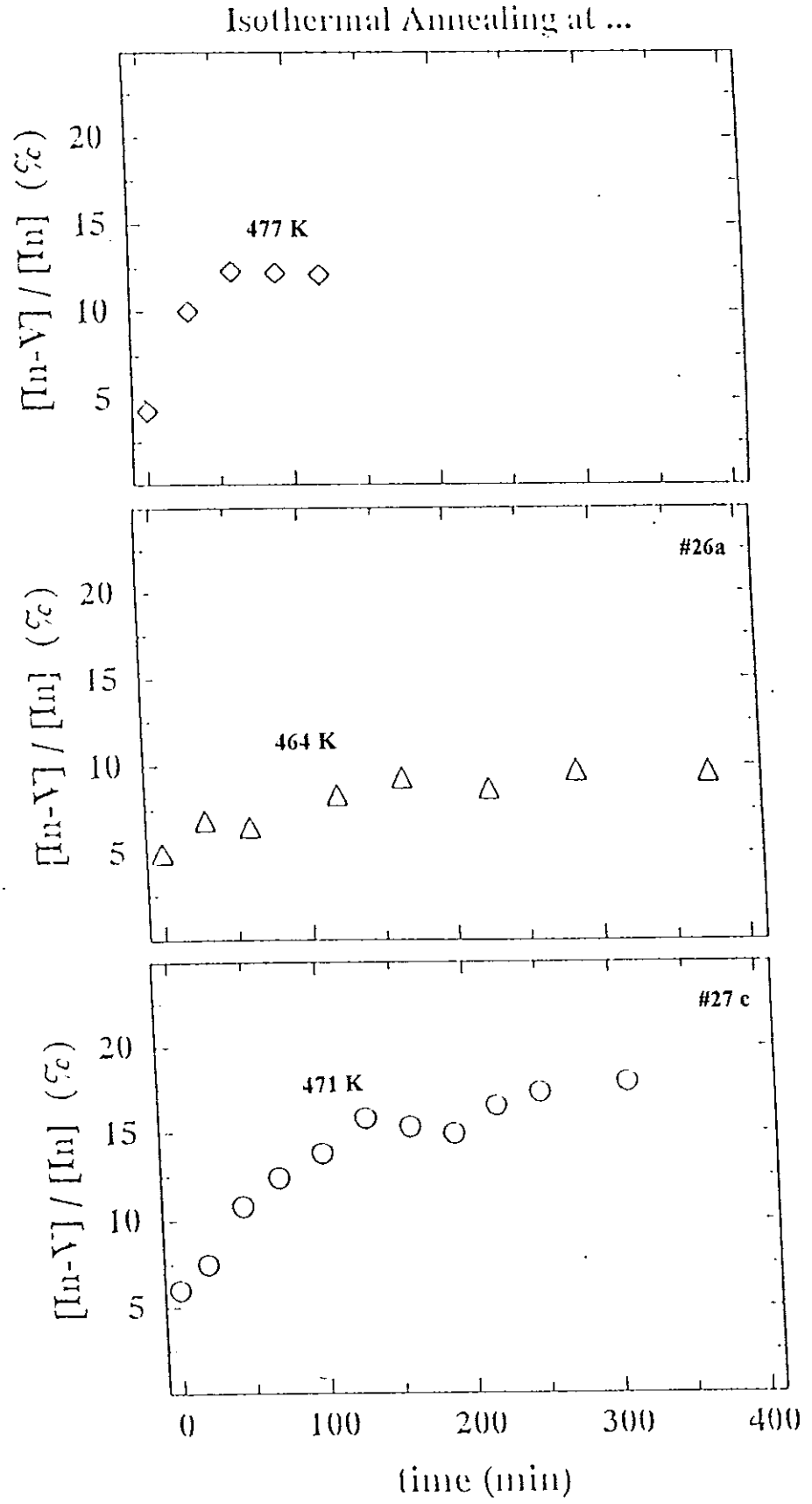

Fig. 29. *Percentage of ^{111}In atoms in In_{Zn}-V'_{Zn} complexes as a function of annealing time for samples annealed at the specified temperatures. All anneals were followed by water quench.*

Under thermal equilibrium conditions the value of the binding energy E_b determines the concentration of In-V pairs. To determine this value, the solution of the rate equation for thermal equilibrium is fitted to the dissociation part of the data of fig.(26) as shown in fig.(31) using the obtained value of the migration energy.

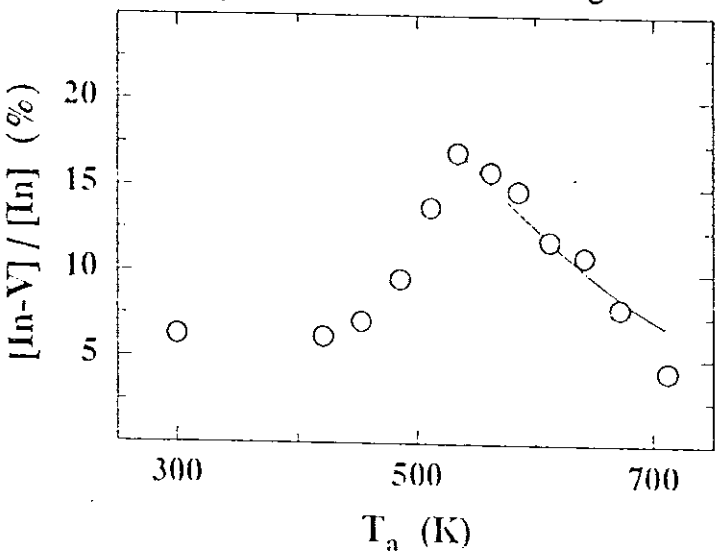

Fig. 31. *Computer fit to the dissociation part of the data of fig. (27).*

From the fit a binding energy of 0.34(0.03) eV is deduced.

Thus, by assuming an attempt frequency of 1×10^{13} s^{-1} the thermal stability of In-V pairs is described by migration energy of 1.30(0.05) eV and a binding energy of 0.34(0.03) eV. However, it is interesting to check whether the deduced values describe well our data.

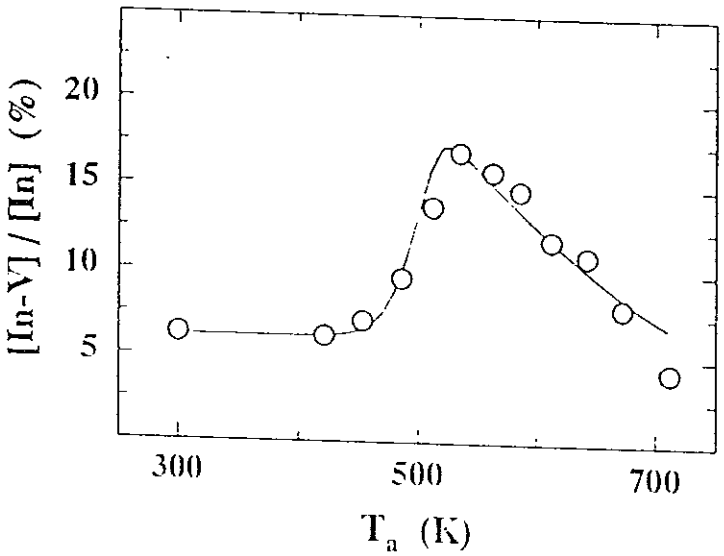

Fig. 32.*Computer fit to the data of fig. (26) for annealing time of 30 min.*

The solid line in fig.(32) represents the fit of the rate equation with the deduced values of E_m and E_b to the data of fig.(26) for annealing time of 30 min. As we can see the solution fits well to our data. Thus, the measured data are well described by the model in the range 300-700 K.

The results on In-V complexes are in remarkable agreement with the recent work of Wichert et al [1]. They found a migration energy of 1.15 eV and a binding energy of 0.35 eV using an attempt frequency of 1×10^{12} s^{-1}. In the same paper they computed their PAC result for migration energy of the metallic vacancy with the ESR data available on the annealing of the metallic vacancy. For ZnSe, E_m = 1.26 eV reported along with ν_0 = 1×10^{16} s^{-1}. Using ν_0 = 1×10^{12} s^{-1} and a temperature of 450 K, the migration energy observed by ESR in ZnSe corresponds to E_m = 0.90 eV. The observed difference between the PAC and ESR data might be caused by the two drastically different attempt frequencies.

4.3.2. Influence Of The Dopant In On The Vacancy Concentration.

In the preceding section the existence of isolated vacancies at low temperature were observed which were attributed to the increase in the pair fraction with annealing time. However, after attaining thermal equilibrium the dissociation of pairs which resulted a decrease in the pair fraction with temperature was observed. Thus, we are interested to know whether the observed decrease in the pair fraction imply a proportional decrease in the local vacancy concentration.

To ascertain what really is happening with the vacancies after dissociation, another experiment for higher temperatures has been carried out. Open circles in fig.(33) show the relative pair fractions measured after heating the ZnSe crystal to the respective T_A for 30 min and subsequently quenched with a high cooling rate, as described in the preceding section.

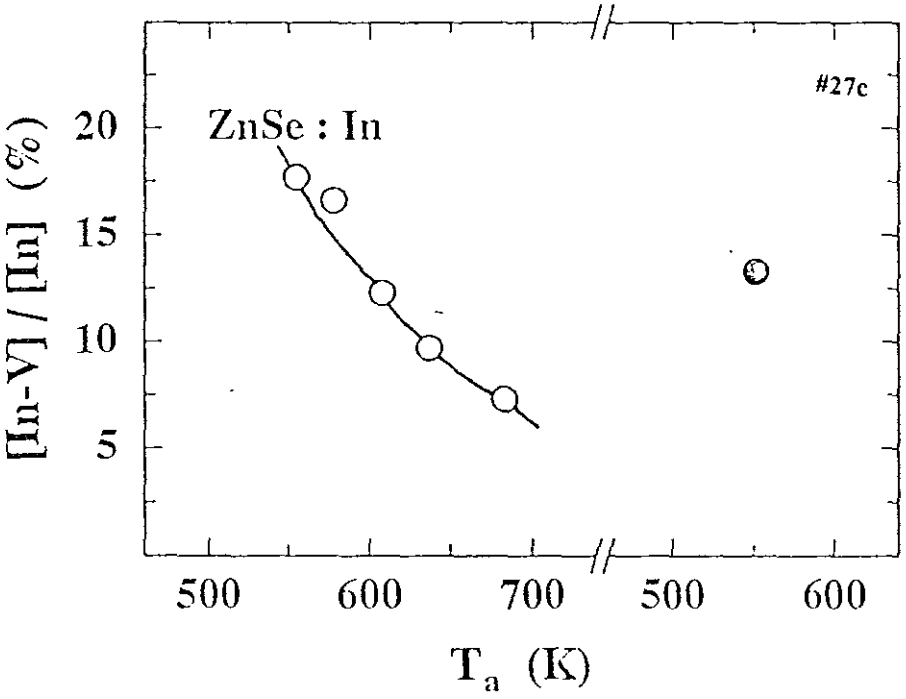

Fig. 33. *Relative fraction of In_{Zn}-V_{Zn} pairs as a function of annealing temperature T_A for 30 min.*

The solid line is, once again, the solution of the rate equation to the data with the reported values of E_m and E_b. It is apparent that the fitted curve describes the data quite well. We therefore, conclude that the values assigned for E_m and E_b are reproducible.

Furthermore, the last data point (closed circle in fig.(33)) was obtained by heating the sample at 554 K for 30 min and water quenched. The observed drastic change in the pair fraction shows that the metallic vacancies are still present in the crystal and thus, the observed decrease in the pair fraction with temperature does not necessarily imply the disappearance of vacancies around the In atoms or a proportional decrease in the local vacancy concentration. However, the measured pair fraction of 0.13 is lower than our expectation value of 0.18 obtained after the fast quench and annealing at the same temperature 554 K. Therefore the question arises, why the pair fraction is too low from our expectation.

In fact, one has to take into account the three days gap between the observation of the two data points. This could definitely lead to a decrease by half in the absolute concentration of In atoms because of its decay with a half life time of 2.8 days.

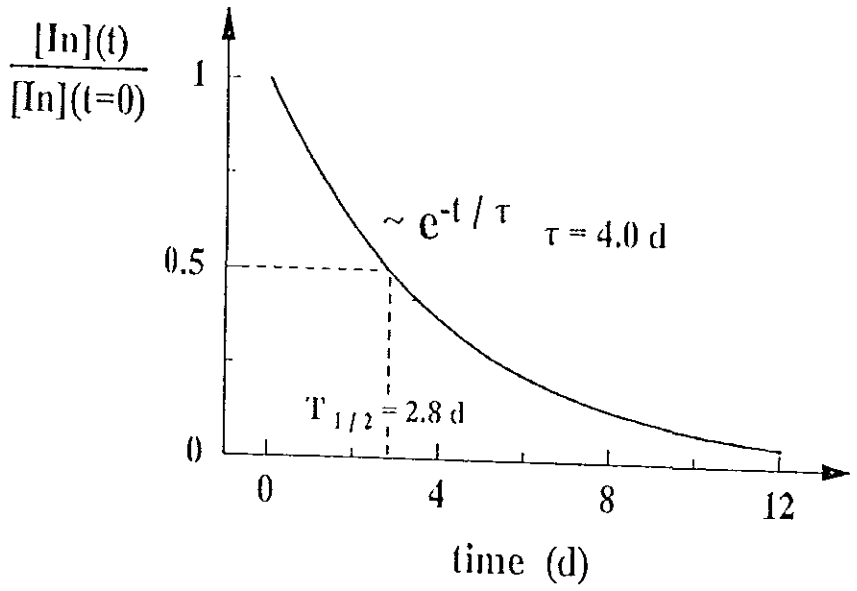

Fig. 34. *Radioactive decay of ^{111}In [44].*

One may thus argue that the change of In concentration might have influenced the vacancy concentration. Notice that we are not concerned with absolute values of defects concentration but only in its local value .

Thus, in order to see whether the decay of In has any influence on the [V], we consider the two extreme boundary conditions for vacancy concentration in solving the rate equation. These are: (a) vacancy concentration stays constant independent of the decay of In or (b) vacancy concentration follows In concentration. In the frame work of our interpretation we expect a minimum of 0.18 to the pair fraction if the vacancy concentration stays constant. However, the observed big difference with our experimental value disregards this possible situation. Whereas, with consideration of the latter boundary condition we expect a pair fraction of about 0.11, quite close to the experimental value.

The present investigation, basically the tendency in the decrease of the pair fraction with the decay of In, favours to the correlation of vacancy concentration to that of the In concentration and thus supports the principle of self-compensation discussed in chapter 2.

However, in solving the rate equation for the investigation of migration energy of the metallic vacancy and it's binding energy with the donor In, the decay of In was not taken into account. Nevertheless, we have observed the influence of In decay on the vacancy concentration. Therefore, the question arises, does the decay of In have any influence on the deduced values for E_m and E_b?

In order to assess to what extent the decay affects the deduced values for E_m and E_b, let us reconsider the data of the previous section based on temperature.

LOW TEMPERATURE CASE

Of course, at low temperatures we have to assume that the vacancy concentration stays constant independent of the decay of In, since the mobility of a vacancy at this temperature does not enable it to leave out of the crystal. The triangles in fig.(35) are the result of the solution of the rate equation to the 464 K data of fig.(29) taking into account the decay of In and the reported values of E_m and E_b. It is quite clear that except for the small deviations observed at the end, the fitted curve describes the data as good as the curve fitted to it in the previous section without considering the In decay. But, the observed small deviations can be attributed to the so-called "***size-effect***" due to the existence of Cd, which is not a matrix atom in the ZnSe crystal. Obviously, the Coulombic pairing that exists between the donor In and the acceptor metallic vacancy breaks as soon as the In decays to Cd. Despite this remarkable fact, the vacancies are still forced to stay around the probe atom due to the larger size of Cd (0.97A°) in comparison to the matrix atom Zn (0.74 A°).

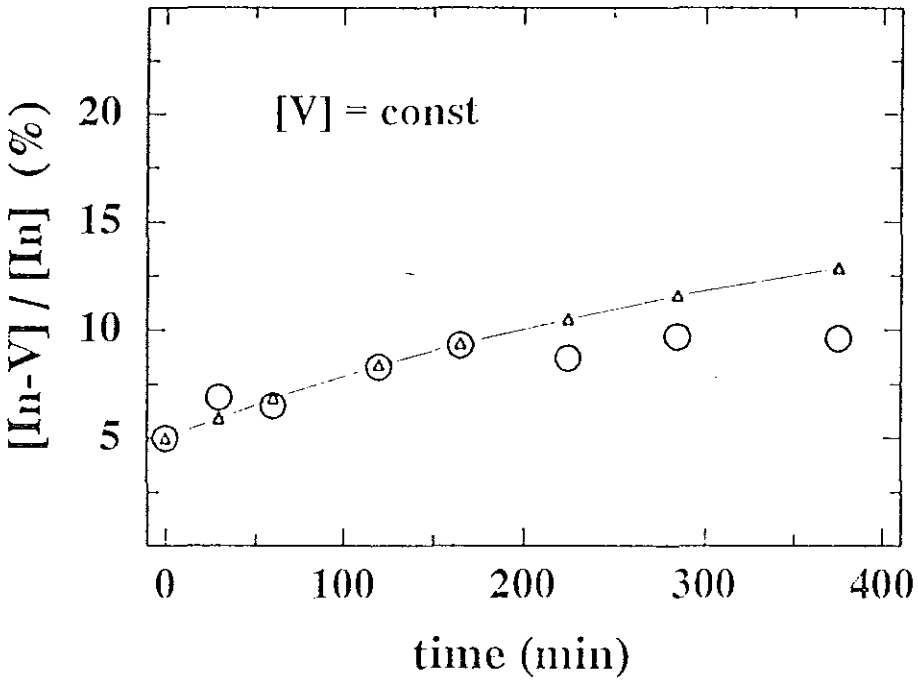

Fig. 35. *Open triangles represent the fit of the rate equation to the isothermal annealing at 464 K with the condition [V] stays constant.*

It is thus plausible to assume that the decay of In has no considerable influence on the measured value of migration energy.

HIGH TEMPERATURE CASE

As it has already been mentioned briefly in the foregoing section, for higher temperatures we have to assume that vacancy concentration follows that of the In concentration. The closed triangles in fig.(36) represent the solution of the rate equation to the data of fig.(26) with the determined values of E_m and E_b and taking into account the decay of In and its subsequent impact on the vacancy concentration. One can easily see that the curve describes quite well the data and thus the decay has no effect on the measured value of binding energy.

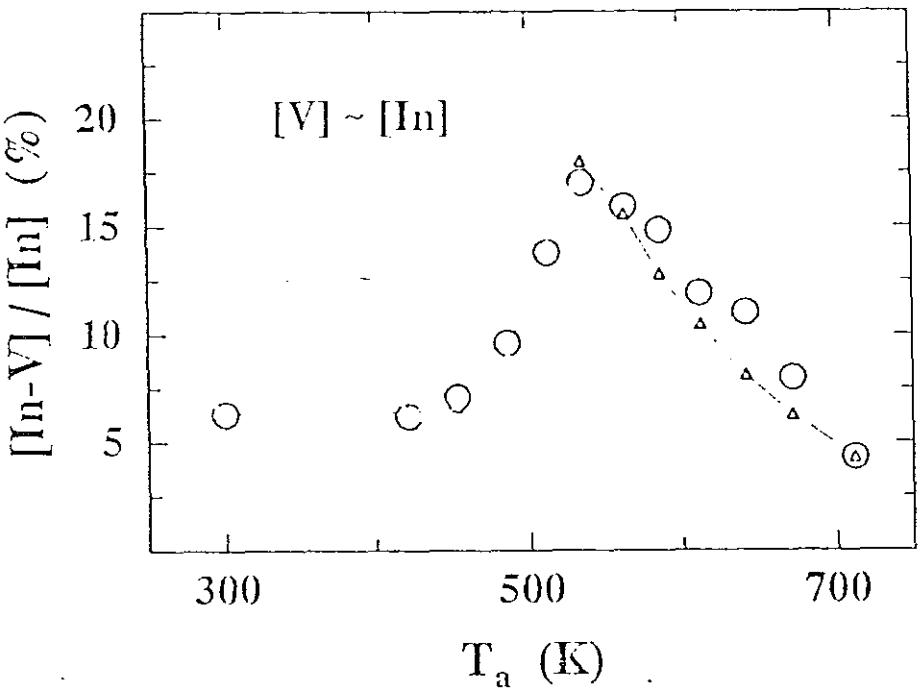

Fig. 36. *The closed triangles represent computer fits to the data of fig. (27) with the condition [V] follows [In].*

In light of the above discussion we conclude that the decay of In has no observable influence on the measured values for migration energy and binding energy in the previous section.

CONCLUSION AND OUTLOOK

We have observed In_{Zn}-V_{Zn} complexes and the presence of isolated V_{Zn} defects in ZnSe using the radioactive ^{111}In in combination with the PAC technique within the temperature range between 300 K and 700 K. The dependence of these complexes on different annealing histories, isothermal annealing and isochronal annealing, helped us in the study of the thermodynamic properties, such as mobility and stability of the metal vacancy V_{Zn} in ZnSe. Annealing at a higher temperature leads to the break-up of these complexes.

The behaviour of the metal vacancy V_{Zn} in ZnSe and its interaction with the donor In_{Zn} is described in a consistent way using a first order rate equation. We have found a migration energy of 1.30 (0.05) eV and a binding energy of 0.34 (0.03) eV for the metal vacancy V_{Zn} assuming an attempt frequency of 1×10^{13} s^{-1}.

In analyzing the data the change of In concentration with time ($T_{1/2}$ = 2.8 d) has been taken into account. The two extreme situations, vacancy concentration stays constant independent of the decay of In and vacancy concentration correlates with In concentration have been considered, and for high temperatures the latter one seems to be more visible. Furthermore, annealing of ZnSe crystal above 700 K causes a decrease in the local vacancy concentration independent of the In decay.

However, to have a better feeling of the behaviour of vacancy concentration in ZnSe crystal with temperature and its relation with the In concentration, other measurements like positron annihilation and Hall effect should be done on ZnSe samples undergone the same treatment to that of our samples.

APPENDIX

All the experimental data reported in Chapter four are the result of three ZnSe samples separately diffused with ^{111}In. Information on the diffusion temperature, diffusion time and other relevant information is given in table I below. Table II shows the measured relative fraction of In atoms involved in the pairing for a given annealing temperature and annealing time for the figures considered in the experimental results and discussion of chapter four.

TABLE I: EXPERIMENTAL DIFFUSION PARAMETERS FOR ZnSe.

Sample No.	Diffusion Temp*. and Se Pressure (mbar)	Temperature for Post-treatment	Data obtained from it
25 a	1070 K, 86	786 K	Fig. (26), Fig. (28)
26 a	1065 K, 86	709 K	Fig. (29) for 477 K Fig. (29) for 464 K
27 c	1068 K, 129	709 K	Fig. (29) for 471 K Fig. (33)

*- The diffusion time for all samples was 15 hours.

TABLE II: experimental values for the fraction of In atoms involved in the pairing as a function of annealing temperature and time.

a) for Fig. 26

Temp. (K)	300	421	453	486	512	535	563	586	612	642	672	712
Fraction (%)	6.3	6 .2	7.1	9.7	13.8	17	15.9	14.8	11.9	11	8	4.3

b) for Fig. 28

Temp. (K)	712 K	783 K	853 K	949 K
Fraction (%)	13.2	8.8	5.3	2.7

c) for Fig. 29. (477 K *Isothermal annealing*)

Annealing time (min)	0	30	60	90	120
Fraction (%)	4.3	10	12.3	12.2	12.1

d) for Fig. 29 (*464 K Isothermal annealing*)

Annealing time (min)	0	30	60	120	165	225	285	375
Fraction (%)	5	6.9	6.5	8.4	9.3	8.7	9.7	9.6

e) for Fig. 29 (*471 K Isothermal annealing*)

Annealing time (min)	0	20	45	70	100	130	160	190	220	250	310
Fraction (%)	6	7.5	10.8	12.4	13.8	15.8	15.3	14.9	16.5	17.4	17.9

f) for Fig. 33

Temp. (K)	555 K	578 K	608K	637 K	683 K
Fraction (%)	17.7	16.6	12.3	9.7	7.3

REFERENCES

1. Th. Wichert, Th. Krings, and H. Wolf: Physica B **185** (1993) 297.

2. Th. Wichert, M. Deicher, G. Grubel, R. Keller, N. Schulz, and H. Skudlik: Appl. Phys. A **48** (1989) 59.

3. Brian Ray, "*II-VI compounds*," Pergamon Press ltd., Headington Hill Hall, Oxford, London, 1969.

4. R. N. Bhargava: J. of Crystal Growth **59** (1982) 15.

5. J. Ren, K. A. Bowers, B. Sneed, D. L. Dreifus, J. W. Cook, Jr., R. M. Kolbas and J.F Schetzina: Appl. Phys. Lett. **57** (1990) 18.

6. M. A. Haase, H. Cheng, J. M. Depuydt, and J. E. Potts: J. Appl. Phys. **67** (1990) 1.

7. Y. Marfing: Prog. Cryst. Growth Charact.: **4** (1981) 317.

8. G. Mandl: Phys. Rev. **134**, A 1070 (1964).

9. D. B. Laks and C. G. Van de Walle: in Ref. 1, P 118.

10. D. B. Laks, C. G. Van de Walle, G. F. Neumark, and S. T. Pantelides: Mater. Science Forum **83-87** (1992) 1225.

11. D. B. Laks, C. G. Van de Walle, G. F. Neumark, and S. T. Pantelides: Phys. Rev. Lett. **66** (1991) 648.

12. C. H. Henry, K. Nassau, and J. W. Shiever: Phys. Rev. B **4** (1971) 2453.

13. T. Sasaki, T. Oguch and H. Katayama-Yoshida: in Ref. 1, P 159.

14. Chris. G. Van de Walle, D. B. Laks, G. F. Neumark, and S. T. Pantelides: Phys. Rev. B **47** (1993) 9425.

15. D. J. Chadi and N. Troullier: in Ref. 1, P 128.

16. D. B. Laks, C. G. Van de Walle, G. F. Neumark, P. F. Blochl and S. T. Pantelides: Phys. Rev. B **45** (1992) 10, 965. And Phys. Rev. Lett. **66** (1991) 648.

17. R. W. Jansen and O. F. Sankey: Phys. Rev. B **39** (1989) 3192.

18. C. Kittel: "*Introduction to Solid State Physics*," 6th. ed. , John Wiley, and Sons, Inc., New York, 1986.

19. E. H. Putley: "*The Hall effect and related phenomena*," Butterworths, London, 1960.

20. S. M. Sze: "*Physics of Semiconductor Devices*," 2d. ed., John Wiley and Sons, New York, 1981.

21. R. A. Colclaser and S. Diehl-Nagle: "*Materials and Devices for electrical Engineers and Physicists*," McGraw-Hill Book Company, New York, 1985.

22. S. Hufner, and E. Mathias: Panal Proceeding Series, IAEA, Vienna, 1972.

23. W. Keppner, T. Klas, W. Korner, R. Wesche, and G. Schatz: Phys. Rev. Lett. **54** (1985) 2371.

24. H. Wolf, Th. Krings, and Th. Wichert: Nuclear Instruments and Methods in Physics Research B **63** (1992) 240.

25. M. Gebhard, B. Vogt, and W. Witthuhn: Phys. Rev. Lett. **67** (1991) 847.

26. R. Keller, M. Deicher, W. Pfeiffer, H. Skudlik, D. Steiner, and Th. Wichert: Phys. Rev. Lett. **65** (1990) 2023.

27. Th. Wichert, E. Recknagel: Microscopic Methods in Metals, ed. by U. Gonser, Topics in Current Physics, Vol. **40** (Springer, Berlin, Heldelberg) 1986.

28. Th. Wichert, N. Achtziger, H. Metzner and R. Sielemann: Hyp. Intro. of Defects in Semiconductors, Ed. by G. Langouche, Belgium, 1992.

29. U. Ott, Diplomarbeit, Universität des Saarlandes, Saarbrucken, Germany, 1993.

30. H. H. Rinneberg: Atomic energy Review **172** (1979) 476.

31. H. Skudlik, M. Deicher, R. Keller, R. Magerle, W. Pfeiffer, P. Pross, E. Recknagel, and Th. Wichert: Phys. Rev. B **46** (1992) 2172.

32. H. Wolf, Th. Krings, U. Ott, U. Hornauer, and Th. Wichert: in Ref. 10, P 1259.

33. H. Metzner, R. Sielemann, S. Klaumunzer, and E. Hunger: Phys. Rev. B **36** (1987) 9535.

34. H. Wolf, U. Hornauer, R. Lermen, Y. Endalamaw, T. Filz, Th. Krings, St. Lauer, U. Ott, E. Singer, M. Tsige, and Th. Wichert: 17th Inter. National Conf. on Defects in Semiconductors **ICDS-17**, Gmunden, July 18-23 1993, Austria.

35. R. Magerle, M. Deicher, U. Desnica, R. Keller, W. Pfeiffer, F. Pleiter, H. Skudlik, and Th. Wichert: Applied Surface Science **50** (1991) 159.

36. EG and ORTEC: Detectors and Instruments for Nuclear Spectroscopy 1991/92.

37. M. Deicher: in Ref. 24, P 189.

38. D. Forkel, N. Achtziger, A. Baurichter, M. Deicher, S. Deubler, M. Puschmann, H. Wolf, and W. Witthuhn: in Ref. 24, P 218.

39. Th. Wichert, M. Deicher, O. Echt, and E. Recknagel: Phys. Rev. Lett. **41** (1978) 1659.

40. G. D. Watkins: Defect Control in Semiconductors (North-Holland 1990) 933.

41. A. W. Harrison: "*Intermediate Atomic and Nuclear Physics,*" St. Martin's Press, New York, 1966.

42. M. Brussler, H. Metzner, K. D. Husemann, and E. Hunger: Phys. Rev. B **38** (1988) 9268.

43. W. C. Hughes, M. L. Swanson, and J. C. Austin: in Ref. 24, P 244.

44. C. Hohenemser, A. Arends, and H. de Waard: Phys. Rev. B **11** (1975) 4522.

45. Norbert Achtziger and Wolfgang Witthuh: Phys. Rev. B **47** (1993) 6990.

46. E. Singer, U. Hornauer, Th. Krings, St. Lauer, U. Ott, H. Wolf, and Th. Wichert: On the existence of Isolated Vacancies in Indium Doped CdS, EuroPhysics Conf. Abstracts, **Vol. 17A**, Sc 27. 27.